CHAOS IN HIGH-POWER HIGH-FREQUENCY GYROTRONS

Markus Airila

Dissertation for the degree of Doctor of Science in Technology to be presented with due permission of the Department of Engineering Physics and Mathematics for public examination and debate in Auditorium F1 at Helsinki University of Technology (Espoo, Finland) on the 6th of February, 2004, at 12 noon.

Helsinki University of Technology
Department of Engineering Physics and Mathematics
Laboratory of Advanced Energy Systems
P.O. Box 2200
FIN-02015 HUT, Finland
Tel. +358 9 451 3198
Fax +358 9 451 3195
Email: markus.airila@hut.fi
Internet: http://www.hut.fi/Units/AES/

ISBN 951-22-6916-3 (printed)
ISBN 951-22-6917-1 (pdf)

ISSN 1456-3320 (printed)
ISSN 1459-7268 (pdf)

Cover: Soini Airila (oil on canvas, 1974)

Otamedia Oy
Espoo 2004

HELSINKI UNIVERSITY OF TECHNOLOGY
P.O. BOX 1000, FIN-02015 HUT
http://www.hut.fi

ABSTRACT OF DOCTORAL DISSERTATION

Author Markus Airila

Name of the dissertation
Chaos in high-power high-frequency gyrotrons

Date of manuscript 16th of January, 2004
Date of the dissertation 6th of February, 2004

☐ Monograph
☑ Article dissertation (summary + original articles)

Department Engineering Physics and Mathematics
Laboratory Advanced Energy Systems
Field of research Fusion and plasma physics
Opponent(s) Professor Klaus Schünemann, Technische Universität Hamburg-Harburg, Germany
Supervisor Professor Rainer Salomaa, Helsinki University of Technology
(Instructor) Professor Olgierd Dumbrajs, Helsinki University of Technology

Abstract

Gyrotron interaction is a complex nonlinear dynamical process, which may turn chaotic in certain circumstances. The emergence of chaos renders dynamical systems unpredictable and causes bandwidth broadening of signals. Such effects would jeopardize the prospect of advanced gyrotrons in fusion. Therefore, it is important to be aware of the possibility of chaos in gyrotrons.

There are three different chaos scenarios closely related to the development of high-power gyrotrons: First, the onset of chaos in electron trajectories would lead to difficulties in the design and efficient operation of depressed potential collectors, which are used for efficiency enhancement. Second, the radio-frequency signal could turn chaotic, decreasing the output power and the spectral purity of the output signal. As a result, mode conversion, transmission, and absorption efficiencies would be reduced. Third, spatio-temporal chaos in the resonator field structure can set a limit for the use of large-diameter interaction cavities and high-order TE modes (large azimuthal index) allowing higher generated power.

In this thesis, the issues above are addressed with numerical modeling. It is found that chaos in electron residual energies is practically absent in the parameter region corresponding to high efficiency. Accordingly, depressed collectors are a feasible solution also in advanced high-power gyrotrons. A new method is presented for straightforward numerical solution of the one-dimensional self-consistent time-dependent gyrotron equations, and the method is generalized to two dimensions. In 1D, a chart of gyrotron oscillations is calculated. It is shown that the regions of stationary oscillations, automodulation, and chaos have a complicated topology in the plane of generalized gyrotron variables. The threshold current for chaotic oscillations exceeds typical operating currents by a factor of ten. However, reflection of the output signal may significantly lower the threshold. 2D computations indicate that stationary single-mode operation of gyrotrons would be impossible if the azimuthal index is about 46 or larger, which is rather close to the presently used values. Moreover, electron beam misalignment can lower this critical value. Above the critical value, less favorable modes suppress the operating mode.

Keywords depressed collector, spatio-temporal chaos, microwave reflections, electron beam misalignment, modeling

UDC
Number of pages 54 + 66
ISBN (printed) 951-22-6916-3
ISBN (pdf) 951-22-6917-1
ISBN (others)
ISSN 1456-3320 (printed), 1459-7268 (pdf)
Publisher Otamedia Oy
Print distribution Advanced Energy Systems, P.O. Box 2200, FIN-02015 HUT, Finland
☑ The dissertation can be read at http://lib.hut.fi/Diss/ 2004/isbn9512269171/

Preface

To write a dissertation is challenging, and plenty of creative pain is needed before the work is finished and publicly defended. Maybe yes, but I personally have evaded many of the painful moments, only because of being lucky to tackle the challenge in the most stimulating atmosphere. After my MSc degree in 2000, it was fully natural to continue working towards the doctoral degree in the Laboratory of Advanced Energy Systems under the Association Euratom-Tekes. I just had to agree with my supervisor, Professor Rainer Salomaa, and my instructor, Professor Olgierd Dumbrajs, what subject I would choose for the dissertation. Luxurious! During the work, Olgierd was always available when I ran into trouble. Rainer's way to supervise me perfectly complemented Olgierd's guidance: with a pertinent remark every now and then, he made me work out many essential, subtle questions which otherwise would have remained as matters of faith.

The content of this thesis reflects many ideas obtained during visits to FZK (Karlsruhe), University of Maryland, and MIT (Boston). I am grateful to Professor Manfred Thumm, Dr Gregory Nusinovich, and Dr Richard Temkin for inviting me to their institutes and arranging seminars solely around my work. After I completed the first manuscript, countless improvements have been done thanks to the pre-examiners Professor Jarmo Hietarinta (University of Turku) and Dr Stefano Alberti (CRPP, Lausanne) as well as Dr Taina Kurki-Suonio, who has carefully read through several versions of the work. The elegantly deLaTeXified layout is due to Dr Marko Santala. My grandfather Soini deserves warm thanks—among many other things—for the nice canvas I used as the basis of the cover picture.

Besides the dissertation, the doctoral degree includes a major and a minor subject. It has been a pleasure to take courses, solve exercises, participate in summer schools, and write assignments with other young scientists Salomon Janhunen, Pia Kåll, Johnny Lönnroth, and Antti Salmi. Special thanks belong to (Dr, to be formal) Tuomas Tala for the endless discussions over lunch which have drawn me into the world of orienteering once and for all.

As an endurance sports enthusiast, I really enjoy belonging to the Finnish fusicist group, where running and cross-country skiing have established as a top-three specialty. Anyway, it always feels good to come home from work greeted with two smiles (one relieved, the other bursting with joy). Auli, you deserve huge thanks for the great job of taking care of our wonderful daughter Laura, me, and our home those days I have been fully immersed in my thesis. I also want to thank my parents, brother, sisters, relatives, and friends for their interest in my work.

Apart from the funding from the laboratory, financial support from the Finnish Foundation for Promotion of Technology, the KAUTE Foundation, and the Jenny and Antti Wihuri Foundation has been most helpful and greatly boosted my motivation. Computing resources for the work have been offered by the Finnish Center for Scientific Computing.

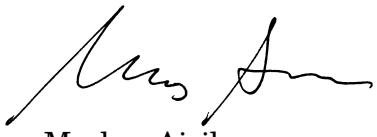

Markus Airila

Original publications

[P1] M. I. Airila, O. Dumbrajs, A. Reinfelds, and D. Teychenné, *Traces of stochasticity in electron trajectories in gyrotron resonators*, Int. J. Infrared Millim. Waves **21**, 1759–1776 (2000).

[P2] M. I. Airila and O. Dumbrajs, *Generalized gyrotron theory with inclusion of adiabatic electron trapping in the presence of a depressed collector*, Phys. Plasmas **8**, 1358–1362 (2001).

[P3] M. I. Airila, O. Dumbrajs, A. Reinfelds and U. Strautiņš, *Nonstationary oscillations in gyrotrons*, Phys. Plasmas **8**, 4608–4612 (2001).

[P4] M. I. Airila and P. Kåll, *Effect of reflections on nonstationary gyrotron oscillations*, to appear in IEEE Trans. Microwave Theory Tech. **52**, No. 2 (February 2004).

[P5] M. I. Airila, O. Dumbrajs, P. Kåll, and B. Piosczyk, *Influence of reflections on the operation of the 2 MW, CW 170 GHz coaxial cavity gyrotron for ITER*, Nucl. Fusion **43**, 1454–1457 (2003).

[P6] M. I. Airila and O. Dumbrajs, *Spatio-temporal chaos in the transverse section of gyrotron resonators*, IEEE Trans. Plasma Sci. **30**, 846–850 (2002).

[P7] M. I. Airila, *Degradation of operation mode purity in a gyrotron with an off-axis electron beam*, Phys. Plasmas **10**, 296–299 (2003).

Most publications selected for this dissertation have more than one author, because the work has been carried out in a research group. M. Airila is the principal author of publications 2, 3, 4, 6, and 7. In the following, his contributions to the joint publications are summarized.

M. Airila calculated the efficiency–smoothness chart of publication 1. For publication 2, he developed the method for calculating gyrotron efficiency taking into account electron trapping, programmed the computer codes, carried out the numerical computations, and participated in writing. He did all programming work and numerical computations related to publication 3 and participated in writing of the article. He developed mathematical models for describing reflections in gyrotrons and wrote the text of publication 4. He performed mode competition calculations for publication 5 and participated in writing. For publication 6, he derived the two-dimensional discretization scheme for the gyrotron equations, implemented it as a computer code, carried out the computations, and participated in writing.

Contents

CHAPTER 1

Introduction

1.1 Global energy needs

Mankind is constantly burning coal, oil, and natural gas in order to produce energy, thus releasing vast amounts of carbon dioxide into the atmosphere. As a result, the global climate is changing. In the coming decades, the rate of climate change will increase owing to the population growth (to some 8.9 billion in the first half of this century [1]) and the rapid economic development among the fastest-growing nations. The world's energy consumption is expected to at least double in various forecasts [2] and scenarios [3], and this increase will be largely covered by fossil fuels, thus boosting the greenhouse effect responsible for global warming.

Extensive efforts against climate change are being pursued by the United Nations in the form of the Kyoto Protocol [4], awaiting for ratification from sufficiently many member states to come effective. The protocol aims at suppressing the greenhouse gas emissions of the parties in 2008–2012 at the level of 5 % below the emissions in 1990. However, implementation of sustainable means of producing energy does not immediately stop global warming. Concrete results follow only after a delay comparable to a human lifespan, since both the global energy system and the relevant atmospheric processes are characterized by great inertia. For example, in order to compensate for the doubling of the world's present electricity consumption of 1.8 TW [5] during 50 years, annually 40 new nuclear reactors of 1 GW or, alternatively, *daily* 200 new wind turbines of 2 MW should be commissioned. At the current rate, no single carbon-free energy source is able to respond to this demand. Indeed, a lot of effort should be put to increase the share of all non-fossil energy sources. In particular, we need to realize that the apparent conflict between nuclear and renewable energy is artificial in the prevailing situation; there is an enormous need for both of them, and they complement each other.

1.2 Nuclear fusion

The release of carbon dioxide is not the sole critical problem of today's energy economy. In the long run, all presently available energy sources will become insufficient. The first step towards a sustainable energy supply should be the departure from the fossil-based economy with the help of renewable and nuclear energy. If accomplished successfully, this would provide mankind with a time-out for taking the second step: replacing the conventional nuclear energy with fusion energy, which is free of the major problems of fission. Fusion energy is released when nuclei of light elements fuse together, whereas fission energy production utilizes splitting of heavy uranium atoms. The easiest fusion reaction occurs between two different hydrogen nuclei, deuterium (D) and tritium (T), which form a helium nucleus and a neutron. The remarkably high reaction energy can be used for electricity production. The deuterium for the reaction can be separated from ordinary water, while tritium is produced in the reactor itself from lithium, which is abundant in the lithosphere. In comparison

to a chemical reaction, a fusion reaction releases roughly a million times as much energy. Therefore, one liter of water is enough to yield the energy equivalent to a barrel of oil, even though there is just one deuterium atom per 6000 hydrogen atoms. With this combination of abundance and energy content of the fuel, fusion will tap a practically inexhaustible energy reservoir. As far as safety is concerned, fusion power plants by their very nature lack the potential for severe reactor accidents. There is but a tiny amount of fuel in the vessel, not containing enough energy to cause destruction. In practice, any malfunction quenches the fusion burn without consequences outside the plant. Moreover, the fusion products are not radioactive, which is a great advantage as regards nuclear waste. The intense neutron flux will, however, activate the reactor structures, but the activity and its half-life can be substantially reduced by choosing proper advanced structural materials. Also tritium is a radioactive substance (half-life about 12 years), which contaminates the vacuum vessel and whose inventories inside the plant require careful bookkeeping. Fortunately, no external tritium transport is required, since the power plant itself will breed the tritium used in fusion reactions.

1.3 Fusion machines

So far, creating favorable conditions for the fusion reaction has been the major challenge on the road to the commercial utilization of fusion energy. The positively charged deuterium and tritium nuclei repel each other because of the electrostatic force, which has to be overcome for the fusion reaction to take place. This can be accomplished by heating the fuel: in the temperature of about 100 million degrees, the nuclei have a sufficient kinetic energy to hit each other in spite of the repulsive force. At such a high temperature electrons escape from the atoms and the fuel becomes a plasma, *i.e.*, a fully ionized gas consisting of charged particles. For net energy yield, it is also necessary to confine the fuel in a sufficient density and thermally well insulated from the surroundings. This is possible using strong magnetic fields. The most successful concept for magnetic confinement is the tokamak [6, 7], a toroidal (doughnut-shaped) device in which the confining helical magnetic field is generated by large external coils together with a strong electric current flowing in the plasma. The plasma current has traditionally been induced using the transformer principle, which allows tokamaks to be operated only in pulses. An alternative toroidal concept, the stellarator, uses more complicated, carefully designed external coils to generate the entire confining field. Since no plasma current is needed in stellarators, they are inherently capable of continuous operation. However, the evolution of stellarators is lagging behind the tokamak branch by about one and a half machine generations. For more information about the largest stellarator experiments, see references 8–11.

Besides tokamaks, stellarators, and other devices relying on magnetic confinement, the possibility to accomplish fusion in small explosions is being investigated. The idea is to use powerful laser beams to compress and ignite solid D-T ice pellets. When the fusion reaction starts, the pellet explodes and flies apart in a tiny fraction of a second. Such a short confinement time could be sufficient for net energy yield thanks to the extreme density achieved, and it is the inertia of the fuel which is responsible for the finite confinement. Therefore, this scheme is called inertial confinement fusion (ICF, see references 12–14).

During the past few decades, the understanding and control of hot fusion plasmas have progressed enormously. The performance of fusion machines is generally measured in terms of the fusion triple product $T_\mathrm{i} n_\mathrm{i} \tau_E$, where T_i is the ion temperature, n_i the ion density, and τ_E the energy confinement time. While in the 1950's the first tokamak experiments achieved values around $10^{14}\,\mathrm{keV\,m^{-3}\,s}$ [15], the largest tokamak today, JET (Joint European Torus, see reference 16) in the United Kingdom, operates close to the so-called break-even conditions with $T_\mathrm{i} n_\mathrm{i} \tau_E \approx 10^{21}\,\mathrm{keV\,m^{-3}\,s}$ and has produced 16 MW fusion power [17]. In the break-even, the fusion power P_fus equals the auxiliary heating power P_aux required to maintain the reaction conditions. Using the energy amplification factor $Q = P_\mathrm{fus}/P_\mathrm{aux}$, this is often expressed as $Q = 1$. An even more challenging goal is to make the fusion reaction sustain itself without any auxiliary heating ($Q = \infty$). This is called ignition, and it requires enhancing the triple product further to $T_\mathrm{i} n_\mathrm{i} \tau_E \gtrsim 5 \times 10^{21}\,\mathrm{keV\,m^{-3}\,s}$. In a power plant reactor, some auxiliary heating will be necessary for current profile control and instability suppression. Thus, an energy amplification factor $Q \approx 30$–40 appears suitable for a commercial reactor in the future.

The above-mentioned results from JET and those from other major tokamaks [18–25] of the world have proven the scientific feasibility of fusion. To demonstrate that fusion is also technologically feasible, a new large-scale experiment is required. To this end, international negotiations for implementing the experimental reactor Iter (the Latin word for "road", see reference 26) and selecting a site for it are presently under way. In Iter, completely new operation regimes will be explored, since the major heating of the plasma comes from fusion products. The reactor is expected to yield $Q \approx 10$ by producing 400 MW of fusion power with 40 MW external power for heating and confinement. The possibility of ignition is not precluded either [27]. Most importantly, Iter will provide a high-irradiation test bench for a variety of technologies. Just to mention a few, the superconducting coils, remote handling systems, and diagnostics must operate reliably in an extremely intense neutron flux. Demonstration of a tritium breeding blanket is also a significant goal for Iter. The first plasma in Iter is expected eight years after the site and construction licenses have been granted.

1.4 Use of radio-frequency waves in plasmas

Consisting of charged particles and being embedded in a strong external magnetic field, a fusion plasma provides an environment where a variety of different waves can exist and several types of instabilities occur. Many wave modes are exploited in plasma heating and current drive, *i.e.*, in transmitting energy and momentum to the plasma particles. These waves span a wide range of frequencies from a few megahertz up to several hundred gigahertz, and they have many differences in excitation, propagation, amplification, damping, and absorption mechanisms. Each wave has its characteristic pros and cons, and sometimes synergic advantages can be obtained by utilizing several heating or current drive mechanisms together.

Three principal radio-frequency (RF) heating schemes are in use in present fusion devices: ion cyclotron (IC), lower hybrid (LH), and electron cyclotron (EC) heating. Ion cyclotron waves in the frequency range 10–100 MHz are absorbed by the ion gyromotion. Consequently, the wave energy is directly deposited to fuel ions. Moreover, efficient generators exist for producing these waves, which has made ion cyclotron

resonance heating the dominant scheme in most tokamaks. However, owing to the wavelength of 3–30 m, large-area launching structures are needed. In addition, they must be located within a few centimeters from the plasma edge to ensure efficient coupling of the wave. Unfortunately, any solid structures in the vicinity of the plasma are potential sources of impurities. Ions other that deuterium and tritium dilute and cool down the plasma. Therefore, even a small impurity concentration can significantly decrease the fusion power.

The frequency range 1–10 GHz corresponds to lower hybrid (LH) waves in tokamak and stellarator plasmas. These waves can be generated with klystrons, which are readily available at the power level needed. Initially proposed for ion heating but failing to perform as expected, LH wave emphasis has shifted to non-inductive current drive. By heating the plasma electrons asymmetrically in the toroidal direction, a net current can be produced and sustained. LH waves have a higher current drive efficiency (measured as the ratio of generated plasma current and launched power) than other non-inductive schemes. The main difficulty in the application of LH waves is the coupling between the antenna and the plasma. As in the case of IC waves, there is a so-called evanescent region in the low-density edge plasma where the waves do not propagate. Therefore, also the LH launcher—often called a "grill"—must be located very close to the plasma.

Electron cyclotron (EC) waves (typically 100–300 GHz) have proven to be suitable for many different purposes in toroidal fusion devices. First, they can provide efficient, well-localized electron heating due to the strong resonance with the cyclotron motion of electrons. Ions are indirectly heated in subsequent collisions with the hot electrons. The electron cyclotron frequency varies with the magnetic field strength in the plasma, which allows controlling the resonance absorption layer. The narrow, pencil-like radio-frequency beam travels almost freely up to the resonant surface where its energy is absorbed by the plasma. Since EC waves propagate also in vacuum, they can be launched from waveguides without contact to the plasma edge. This protects the launching structure from the harsh environment and prevents impurity accumulation in the plasma. Thanks to their small cross section, the EC wave launchers require little vessel surface. Therefore, better coverage of the plasma by the energy-producing and breeding blankets, vital in power reactors, becomes possible. Moreover, thanks to their low attenuation in waveguides or quasi-optical transmission lines, EC waves can be generated in relatively distant sources, which can therefore be positioned out of reach of the damaging neutron irradiance.

In addition to electron cyclotron resonance heating (ECRH), electron cyclotron current drive (ECCD) is an important application of EC waves. A tokamak relying on inductive current can only be run in pulses, since the current in the central solenoid can not be constantly increased. However, the possibility of a steady-state tokamak is seriously investigated. In such a machine, EC waves along with LH waves and neutral beam injection (NBI) could be used to replace the inductive current drive. The results are encouraging: a fully non-inductive plasma current in a tokamak has been transiently sustained with ECCD in the Japanese WT-2 [28] and WT-3 [29], the Russian T-10 [30], and in steady state in the Swiss tokamak TCV [31]. In comparison to LH waves and NBI, the advantage of EC waves in current drive lies in their highly localized absorption, which allows accurate current profile control. In particular, it is possible to stabilize neoclassical tearing modes (NTM's) by restoring the plasma

FIGURE 1.1. *140 GHz prototype gyrotron for W7-X (fabricated by Thales Electron Devices, Vélizy). [33]*

current in magnetic islands with ECCD. These tasks will play an important role in the application of ECCD in Iter [32].

1.5 The gyrotron

While IC and LH waves can be routinely used in fusion experiments, the development of powerful EC wave sources is still in progress. The only microwave source capable of generating power levels relevant for fusion in this frequency range is called the *gyrotron*. The name derives from the words "gyrating electron", pointing to the physical phenomenon central for the operation. The appearance of an operating gyrotron is dominated by magnets, cooling systems, power connections, and shielding, so that the vacuum tube itself is completely hidden. Figure 1.1 shows the stripped-down 140 GHz prototype gyrotron for the new stellarator Wendelstein 7-X, to be built in Greifswald, Germany. Figure 1.2 depicts schematically the main components of a gyrotron with a depressed potential collector. Gyrotron operation is briefly summarized in this section. More details are available in several books that have been published on gyrotrons. Russian ones [34, 35] contain much of the original work. In English, perhaps the most thorough exposition can be found in reference 36. The collections 37–39 concentrate more on applications.

Gyrotron converts the energy of an accelerated electron beam into electromagnetic radiation. The conversion takes place in an evacuated metallic cavity embedded in a strong magnetic field, which makes the electrons revolve around the field lines at the cyclotron frequency ω_c and, consequently, emit *bremsstrahlung*, as does any electric charge in accelerated motion. In addition, the beam interacts with the transverse

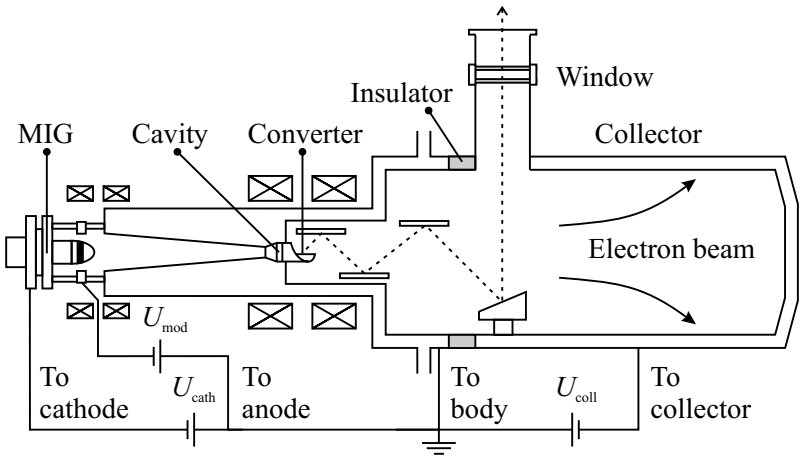

FIGURE 1.2. *A schematic layout of a gyrotron with a depressed potential collector and radial output. The wave energy is extracted from electrons which have been accelerated with a magnetron injection gun (MIG). The wave is generated in a specially designed interaction cavity (resonator), which can sustain oscillations on the desired frequency. In modern gyrotrons, the specific mode generated in the resonator is converted by a mode converter into a Gaussian beam, which is directed with special mirrors out of the gyrotron through a diamond window. The decelerated electron beam, instead, is separated from the wave and dumped onto a collector, where its residual energy is dissipated.*

electric field, which rotates at the resonator eigenfrequency ω. However, if the electrons radiate independently of each other, the resulting net radiation field is zero because of the superposition of waves in random phases. To induce phase correlation between electrons, gyrotrons elegantly utilize the relativistic dependence of the cyclotron frequency on the electron energy: the more energetic (massive) the electron, the slower it rotates. Assuming that the magnetic field in the cavity has been tuned so that the cyclotron frequency equals the eigenfrequency of the operating mode, $\omega_c = \omega$, the electrons experience in their own frame of reference a constant electric field that either accelerates or decelerates them depending on the relative phase of rotation. The changes in energy immediately imply opposite changes in cyclotron frequency, and eventually all electrons become bunched in the "neutral" phase of the electric field, emitting coherent bremsstrahlung.

While the bunching mechanism is essential for the coherence of the emitted cyclotron radiation, it does not guarantee net energy transfer from the electron beam to the electromagnetic wave. Indeed, any energy the wave gains by decelerating electrons is balanced by an energy loss due to a symmetrically accelerated electron population. Positive energy balance can still be obtained by introducing a frequency mismatch between the wave and the electron cyclotron motion. If the wave rotates slightly faster than the electrons, the bunch lags behind the electric field and is constantly decelerated.

The main driving force for high-power gyrotron development comes from fusion, which is constantly demanding more and more intense microwaves. Recently, the performance of gyrotrons has achieved a level which allows applying them to produce high-power microwaves for plasma heating, current drive, and profile control. Since the invention of the gyrotron operation principle in 1959 [40–42], many theoretical and technological problems have been solved. Operation at the higher harmonics

of the cyclotron frequency was demonstrated in 1963. The fundamental operating frequency was significantly increased when superconducting magnets became available [43]. Major efficiency improvement has been achieved with the implementation of depressed collectors [44–46]. Most recently, advances in the development of chemical vapor deposition (CVD) diamond windows [47] have allowed transmission of megawatt-level continuous-wave beams out of the vacuum tube. At present, the "world record" performance has been set with the 140 GHz gyrotron [48] for W7-X. This gyrotron has produced an output power of 850 kW for three minutes [49]. For Iter, 20 MW of ECRH power at 170 GHz is planned in the first phase [50], which in the present design is to be realized with tubes of 1 MW each. An economically very attractive alternative would be to use more powerful, 1.5–2 MW gyrotrons if they were available. To this end, a development program for advanced coaxial cavity gyrotrons is being carried out as an Iter task at the Forschungszentrum Karlsruhe (FZK), Germany. The upper power limit for conventional resonators seems to be around 1 MW, above which either Ohmic heating damages the cavity or, alternatively, the resonator diameter must be made so large that mode competition becomes intolerable. In the so-called coaxial cavities mode competition is relieved with a corrugated metallic insert in the cavity. Coaxial cavity gyrotrons have proven their potential to reach 2 MW in long-pulse or continuous operation [51–57]. Another currently active field of research is stepwise frequency-tunability [58]. Tunable gyrotrons will provide enhanced flexibility in the localization of the EC power absorption, and they can be used for controlling instabilities [59]. The feasibility of frequency tunable gyrotrons has been preliminarily demonstrated in experiments [60–62].

1.6 Chaos in gyrotrons

Many completely deterministic dynamical systems can exhibit apparently irregular and unpredictable behavior. This phenomenon is called *deterministic chaos*: There are equations which govern the evolution of the system, making it deterministic. However, the solutions of the equations are extremely sensitive to the initial conditions, *i.e.*, chaotic. Because of the strong Russian contribution to this field, the word "stochastic" is used as a synonym for "chaotic" in publications 1–7 (as opposed to the Western convention, in which stochasticity contains the idea of randomness instead of determinism). Chaos can exist only in sufficiently complex systems. If the equations of the system are written as a set of N autonomous first-order differential equations, the following conditions are necessary for chaos [63]:

- The system is nonlinear.
- $N \geq 3$.

Apparently, many everyday systems fulfill these conditions. Common examples of systems showing chaotic dynamics are, *e.g.*, a double pendulum, a dripping faucet, and weather.

It is very useful to work in *phase space* when analyzing dynamical systems. The phase space of an M-dimensional system is spanned by a set of generalized coordinates q_i ($i = 1, \ldots, M$) and their derivatives $\mathrm{d}q_i/\mathrm{d}t$ (generalized momenta). Hence, the phase space is $2M$-dimensional, and the state of the system is described by a

single point, possibly traveling along an orbit. It is illustrative to compare the behavior of two nearby orbits of a chaotic system with two raisins in a dough. When the baker kneads the dough, stretching and folding it, the raisins come soon apart, no matter how close to each other they initially were located. Similarly, the phase space orbits of a chaotic system experience continuous stretching and folding, which separate nearby orbits exponentially. In the long run, the orbits may again end up in the same region, but it is the everywhere prevailing exponential divergence in short times that is most characteristic for chaotic dynamical systems. Such common criteria of chaos as the sensitive dependence on initial conditions or completely random-looking motion stem from this property [64].

Gyrotron operation includes several nonlinear dynamical processes, so one should be aware of possible chaotic behavior of gyrotrons. In particular, the electron beam current is a potential bifurcation parameter, that is, the operation might turn from regular to chaotic when a certain threshold value for the current is exceeded. Since this possibility is closely related to the attempts to increase the unit output power, it is relevant to ask whether the present development is approaching such a threshold. In this thesis, three different chaos scenarios are distinguished: chaotic electron trajectories, chaotic radio-frequency signal, and spatio-temporal chaos in the resonator field structure. The aim of the study is to assess their relevance to high-power gyrotron development.

1. *Chaotic electron trajectories.* Collector potential depression is used to improve gyrotron efficiency and to suppress heat deposition and x-ray generation on the collector. The energy recovered from the electron beam is proportional to the collector voltage. However, the voltage is limited by the smallest longitudinal energy of the electrons, which should not be reflected back to the interaction cavity. Therefore, efficient usage of depressed collectors requires good knowledge of the residual energy spectrum of the spent electron beam. During their passage through the interaction cavity, the electrons might end up into chaotic orbits. In such a case their residual energies after the interaction could not be theoretically predicted. Consequently, the design and efficient operation of depressed collectors would be jeopardized.

2. *Chaotic radio-frequency signal.* Striving for higher output power, it is required that higher beam currents can be used. This could drive the gyrotron into an operating regime of chaotic oscillations. From the viewpoint of fusion applications, it is important that the output signal is powerful and monochromatic. Emergence of chaos would decrease the power, because efficient energy transfer from the beam to the electromagnetic wave requires an optimized field distribution in the resonator. Also the spectral purity of the signal would deteriorate, leading to a reduction in mode conversion, transmission, and absorption efficiencies.

3. *Spatio-temporal chaos.* To keep the Ohmic heating of resonator walls within acceptable limits, highly overmoded large-diameter cavities and high-order TE_{mp} modes (large m) must be used in high-power gyrotrons. It is possible that the transverse symmetry of the RF field breaks down for high m, rendering the field structure chaotic both in space and time. This would cause similar problems as the purely temporal chaos discussed above.

Chaos in electron trajectories during gyrotron-type of interaction has been studied in reference 65 with the Hamiltonian method assuming a plane wave electromagnetic field. It was found that relativistic effects prevent the onset of chaos in this simple model. In reference 66 it was mathematically shown that a Gaussian-type axial field profile can lead to transient chaos. In an infinitely long resonator the trajectories can be much more complicated [67]. This result leaves the question about chaos in realistic resonators completely open. In publication 1, the powerful Hamiltonian method is applied to realistic gyrotron resonators: a finite interaction cavity with a true longitudinal field profile. In publication 2, depressed collectors are investigated using some of the methods of publication 1.

Chaotic radio-frequency oscillations in gyrotrons were theoretically found in references 68–70, and the operating parameter plane was roughly divided into regimes of stationary and nonstationary oscillations. In publication 3, a more straightforward numerical method for analyzing the equations in question was developed and implemented into computer codes. A detailed chart of oscillation regimes (stationary, automodulation, chaos) was generated. Publication 4 extends this study to include reflections of microwave power back into the cavity—a problem which has recently been studied by many other research groups as well [71–74]. Publication 5 deals with the effect of reflections on the coaxial gyrotron for Iter.

The two-dimensional theory of nonstationary gyrotron oscillations was developed in references 75 and 76. In those articles, the equations were solved with the method of characteristics, and results were provided for one particular combination of operating parameters. In publication 6, a method for direct numerical solution of the equations was developed. The critical azimuthal index m_{crit}, above which stationary single-mode operation breaks down, was calculated in the whole relevant region of the operating parameter plane. In publication 7, the analysis was extended to include possible misalignment of the electron beam.

This thesis is organized as follows: In the beginning of chapter 2, some tools for detecting and quantifying chaos and related nonstationary processes are reviewed. Chapter 2 also contains a concise derivation of the equations which constitute the theory of nonstationary processes in gyrotrons and are therefore of central significance in this thesis. The numerical methods used for solving these equations are presented. In chapter 3, which is a somewhat modified version of the review article [77], electron trajectories and nonstationary behavior of gyrotrons are analyzed using the tools presented in chapter 2. Chapter 4 contains a summary and discussion. The original publications [P1–P7] can be found at the end of the thesis.

CHAPTER 2

Methods

2.1 Characterization of nonstationary behavior

In this section, some tools for detecting and quantifying chaos and other types of nonstationary behavior of dynamical systems are briefly reviewed. The methods will be applied to the solutions of the gyrotron equations presented later in this chapter. More details on characterization of nonstationary behavior can be found, *e.g.*, in references 63, 64, and 78.

2.1.1 Routes to chaos

Chaotic behavior usually requires the system parameters to lie in a specific range, otherwise the motion is regular. As the parameters are varied, the transition from regular motion to chaos occurs through a sequence of *bifurcations*; events which change the structure of the phase space. In general, only quantitative changes of the system behavior result from small variations of a parameter. For some critical parameter values, however, a small variation results in a qualitative change in the phase space orbits. These critical values are called bifurcation values. Different sequences of bifurcations are referred to as the routes to chaos. There exists a well-developed but by no means complete theory, which can explain many phenomena observed in connection to different routes; however, it lies beyond the scope of this thesis (see, *e.g.*, reference 64).

Period doubling is perhaps the most famous route to chaos. Transition from a stationary state into chaos along with variation of a system parameter μ takes place through a series of period doublings at $\mu = \mu_1, \mu_2, \ldots$. The period doubling bifurcations occur with diminishing intervals of the bifurcation parameter, and rather universally, the sequence of bifurcation parameters converges to the limit

$$\lim_{i\to\infty} \frac{\mu_{i+1} - \mu_i}{\mu_i - \mu_{i-1}} = \frac{1}{\delta} = \frac{1}{4.6692\ldots}, \tag{2.1}$$

where δ is called the Feigenbaum's constant (see, *e.g.*, reference 63).

In many systems, an initial transient period of irregular motion precedes the settling into the regular—stationary or periodic—orbit. If the duration of this transient is observed to increase, eventually to infinity, as a system parameter is varied, the system is said to follow the so-called *transient route* to chaos.

Intermittency resembles the transient route with the difference that intermittent chaotic sequences appear repeatedly within otherwise regular motion. Before the transition into completely chaotic motion, the average duration of the chaotic sequences increases and, correspondingly, the regular periods in between become shorter. In spite of their similarity, intermittency can be regarded as a more dangerous (consider the vibrations of an airplane, for example) route than the transient one. Indeed, an unpredictable chaotic burst can in principle occur at any instant, no matter how long the system has exhibited apparently regular behavior.

Finally, the *quasiperiodic route* manifests itself through the following series of bifurcations: stationary state → periodic motion → quasiperiodic motion → chaos. The second bifurcation induces another fundamental frequency, which is incommensurate with the first one, that is, their ratio is irrational. The third bifurcation would introduce still another fundamental frequency, but the resulting quasiperiodic orbit is typically unstable; as a result, the system becomes chaotic.

2.1.2 Poincaré map

Useful information about a dynamical system can be obtained with the help of the so-called Poincaré map. Such a map is constructed by plotting two components of the state vector of the system versus each other at discrete times. If an external periodic force acts on the system, it is natural to choose the time interval of points to coincide with the period of the force. Otherwise, the interval can be chosen by other means [64].

The appearance of a Poincaré map is very simple for regular motion: a stationary orbit is mapped as a single point, and n-periodic orbits as n points. Furthermore, quasiperiodic motion fills out a closed curve, and chaotic motion manifests itself as a *fractal*, a set consisting of an infinite number of points but not having a well-defined boundary. The topological dimension of a fractal is not an integer number. The power of Poincaré maps is the apparent visual difference of these types of figures, making it possible to easily distinguish between various types of motion.

2.1.3 Signal processing techniques

Fourier transform is one of the most commonly used tools in signal processing. As the transform sorts a signal according to its frequency components, it is very useful in determining possible chaos. In particular, a quasiperiodic signal might seem chaotic at first glance, but its Fourier spectrum reveals that there is only a set of discrete frequencies present. Meanwhile, a chaotic signal has a broad continuum spectrum with spikes at the dominant frequencies. One should be aware, however, that a continuum may result from merging of several discrete frequency peaks in a system with very many degrees of freedom. Another non-chaotic cause of continuous spectra is the possible noise in the signal.

Cross-correlation R_{AB} of two signals $A(t)$ and $B(t)$ over a time interval $[t_1, t_2]$ is defined as

$$R_{AB} = \frac{1}{t_2 - t_1} \int_{t_1}^{t_2} A(t)B(t)\,\mathrm{d}t. \tag{2.2}$$

It is assumed here that the signals have been linearly transformed to have averages $\langle A(t)\rangle = \langle B(t)\rangle = 0$ and variances $\sigma_A^2 = \sigma_B^2 = 1$. As a special case, one can use the same signal for both $A(t)$ and $B(t)$, one of which is delayed by a time T. The resulting function of T is the autocorrelation function of the signal,

$$R_A(T) = \frac{1}{t_2 - t_1 - T} \int_{t_1+T}^{t_2} A(t)A(t-T)\,\mathrm{d}t. \tag{2.3}$$

The value of the autocorrelation function is always unity for $T = 0$. For positive delay $T > 0$, it can reach unity only if the signal is perfectly periodic—in this case

$R(nP) = 1$ for all integer multiples of the period P. Moreover, autocorrelations of chaotic and random signals are essentially different: if $A(t)$ is chaotic, $R_A(T)$ decays exponentially for $T > 0$, whereas $R_A(T)$ of a random $A(t)$ drops close to zero when T becomes large enough.

2.2 Gyrotron equations

2.2.1 Historical background

This section describes the simple dimensionless form of gyrotron equations which are based on Maxwell's equations and weakly relativistic laws of motion. The consideration is limited to operation at the fundamental cyclotron frequency. Historically, the development of gyrotron theory has progressed in several steps: The averaged equations of electron motion in a cold-cavity field were reported by Yulpatov in 1966 [79, 80]. In 1973, an article was published, where the RF field was treated in a self-consistent manner [81], allowing the electron beam to influence the axial field profile (see also reference 82). Next, in 1981, the axial profile was again held fixed and, instead, the azimuthal structure of the field was considered beam-dependent [83]. Up to this stage of the development, all work was carried out assuming a stationary state. A self-consistent time-dependent theory of gyrotron oscillations was published in 1986 together with some analysis of the corresponding equations [68–70]. Here, again, the transverse structure of the RF field was assumed fixed and, in particular, it was represented as one of the TE (transverse electric field) modes of a circular waveguide. Finally, in 1989, this representation was generalized to a description in which both the axial and the transversal structure of the field were beam-dependent, having a smooth envelope allowed to evolve in time self-consistently [75, 76]. This most recent theory has particular relevance in connection with gyrotrons having overmoded large-diameter cavities prone to mode competition.

2.2.2 Scope of application

Gyrotron belongs to the family of cyclotron resonance masers (CRM's), which all utilize the same bunching mechanism to extract energy from the magnetized electron beam. However, the electron beam becomes resonant with an essentially different electromagnetic wave in each of the devices. While gyrotrons operate near cut-off (the phase velocity is much greater than c), gyro-backward-wave oscillators (gyro-BWO's) utilize a backward-traveling wave, and in gyro-traveling-wave tubes (gyro-TWT's) and cyclotron autoresonance masers (CARM's) the phase velocity is somewhat larger and almost equal to c, respectively. Accordingly, each device has its characteristic properties: Gyro-BWO's can be rapidly tuned over a wide frequency range, but they provide relatively low efficiency. Gyro-TWT's amplify an input signal to a high-power broadband signal with high efficiency. CARM's take advantage of the Doppler shift of the wave frequency to maintain the resonance in spite of the variation of the gyrofrequency during the interaction. The Doppler shift also lowers the magnetic field needed to obtain the desired output frequency. For more detailed descriptions of gyro-BWO's, gyro-TWT's, and CARM's, see, *e.g.*, reference 84 and the extensive list of references therein. In this thesis, operation near cut-off is assumed, limiting the

scope of application to gyrotrons—which are most attractive from the perspective of fusion energy research thanks to their high-power capability.

The existence of different characteristic time scales makes it possible to simplify some parts of the gyrotron equations. First of all, an electron performs a cyclotron rotation in a few picoseconds while it needs some hundreds of picoseconds for traversing the gyrotron cavity. This is exploited by averaging the equation of motion over the fast cyclotron rotation. In the numerical computations, this approach allows one to take time steps which are a fraction of the cavity transit time and not a fraction of the cyclotron period. Furthermore, if the transit time of electrons is short in comparison to the time constant of the cavity, the electrons experience an essentially fixed axial distribution of the field as they traverse the cavity. Under these circumstances, the interaction can be modeled by periodically launching an ensemble of electrons and following their motion in the fixed field. The electromagnetic source and the evolution of the field can then be deduced from the current resulting from the motion of electrons. The assumption of fast transit is good except in the very extreme cases where the modulation period of the field becomes comparable to the transit time.

At high beam current, the charge density in the beam tunnel and resonator may become so large that the effective accelerating voltage decreases and beam instabilities can occur (see, *e.g.*, references 85 and 86). This leads to an increase in the energy and velocity spreads of the electrons and, consequently, decreases the efficiency. Proper treatment of these effects is a separate, formidable task which lies beyond the scope of this thesis.

2.2.3 Equation of motion for electrons

Electron bunching, which is of central importance in gyrotrons, is caused by the relativistic mass increase of the electrons. Therefore, a purely classical description could not be used to describe gyrotron interaction. However, a relativistic expression is needed only for the electron cyclotron frequency $\omega_\mathrm{c} = eB/\gamma_\mathrm{rel} m_\mathrm{e}$ when it appears in the difference $\omega - \omega_\mathrm{c}$, since all other relativistic effects can be neglected in typical gyrotrons with the accelerating voltage $U_\mathrm{cath} < 100\,\mathrm{kV}$. (The rest mass of electron corresponds to the energy of $m_\mathrm{e}c^2 = 511\,\mathrm{keV}$, so the relativistic factor $\gamma_\mathrm{rel} = 1 + eU_\mathrm{cath}/m_\mathrm{e}c^2 < 1.2$.) The resulting theory can be regarded as weakly relativistic: a first-order Taylor expansion for ω_c is sufficiently accurate. The derivation given here follows reference 87, which can be consulted for additional details.

In a gyrotron resonator, the magnetic field is axial, $\mathbf{B} = B\mathbf{e}_z$, and the rotating electric field $\mathbf{E}$ transversal. The electric field intensity is typically of the order of $10^6\,\mathrm{V/m}$, resulting in a quiver velocity $v_\mathrm{q} = eE/\omega m_\mathrm{e}$ of about $10^{-3}c$. The interaction of the electrons with the magnetic component of the wave is v_q/c times weaker than with the electric component and can clearly be neglected. Accordingly, the axial momentum $\mathbf{p}_\parallel$ remains constant under the influence of the Lorentz force of the electromagnetic fields, and the equation of motion is

$$\frac{\mathrm{d}\mathbf{p}_\perp}{\mathrm{d}t} = -e(\mathbf{E} + \mathbf{v} \times \mathbf{B}) \qquad \Longleftrightarrow \qquad \frac{\mathrm{d}\mathbf{p}_\perp}{\mathrm{d}t} + \omega_\mathrm{c}\mathbf{p}_\perp \times \mathbf{e}_z = -e\mathbf{E} \tag{2.4}$$

together with $\mathbf{p}_\parallel$ = constant. The latter form of equation (2.4) is obtained by expressing the transverse velocity $\mathbf{v}_\perp$ and magnetic field $\mathbf{B}$ in terms of the transverse momentum, $\mathbf{p}_\perp = m_\mathrm{e}\mathbf{v}_\perp$, and the cyclotron frequency of electrons, respectively.

In a waveguide with a slowly varying cross section near the cut-off of the wave, the dependences of the electric field on axial, transverse, and time coordinates can be separated:

$$\mathbf{E}(\mathbf{r},t) = \mathrm{Re}\,[F(z,t)\mathbf{E}_\mathrm{t}(r,\varphi)\mathrm{e}^{\mathrm{i}\omega t}], \tag{2.5}$$

where ω denotes the output frequency (the eigenfrequency of the mode) and $\mathbf{E}_t$ is dimensionless. The electrons traverse the cavity fast enough to experience an essentially fixed field profile, so that actually $F = F(z)$ in this context. [The time dependence of F is taken into account when the evolution of the field is considered in section 2.2.4. The field evolves in the very slowest time scale which is measured by the dimensionless time τ defined below in equations (2.10).] Moreover, the transverse structure of the field is close to the eigenmode of the waveguide and is determined in a fixed cross section $z = z_0$ by the Helmholtz equation

$$\nabla_\perp^2 \mathbf{E}_\mathrm{t} + \frac{\omega(z_0)^2}{c^2}\mathbf{E}_\mathrm{t} = 0 \tag{2.6}$$

with the boundary condition that the tangential field must vanish at the conducting wall. The cross section of a conventional gyrotron cavity is circular; in this case the solution is given by the Bessel function J_m (see reference 88 for details):

$$\mathbf{E}_t(r,\varphi) = E_r\mathbf{e}_r + E_\varphi\mathbf{e}_\varphi = \left[\frac{\mathrm{i}m}{\kappa r}J_m(\kappa r)\mathbf{e}_r - J_m'(\kappa r)\mathbf{e}_\varphi\right]\mathrm{e}^{\mathrm{i}m\varphi}, \tag{2.7}$$

where the transverse wave number is $\kappa = \omega(z_0)/c$, and φ can be set arbitrarily, since the electron momenta will always be averaged over all phases of rotation. The so-called cut-off frequency $\omega(z) = \nu c/R(z)$ of the waveguide is the lowest propagating frequency; it depends on the waveguide radius $R(z)$ and the mode eigenvalue ν.

Introducing the complex notation $P = p_r + \mathrm{i}p_\varphi$ for the transverse momentum, and similarly, $E = E_r + \mathrm{i}E_\varphi$, the vector equation (2.4) can be written as

$$\frac{\mathrm{d}P}{\mathrm{d}t} - \mathrm{i}\omega_\mathrm{c}P = \mathrm{i}eEF(z)\mathrm{e}^{\mathrm{i}\omega t}. \tag{2.8}$$

We also define a slowly varying variable $\tilde{P}$ by the relation $P = \tilde{P}\exp(\mathrm{i}\omega t)$ and note that J_m and J_m' combine into J_{m+1}. The evolution of $\tilde{P}$ in a time scale much slower than $1/\omega$ is then given by the equation

$$\frac{\mathrm{d}\tilde{P}}{\mathrm{d}t} + \mathrm{i}(\omega - \omega_\mathrm{c})\tilde{P} = \mathrm{i}eF(z)J_{m+1}(\kappa R_\mathrm{el}), \tag{2.9}$$

where R_el is the radius of the hollow electron beam. As mentioned above, the cyclotron frequency ω_c in (2.9) can be expanded as a Taylor series (first order in β^2) about the nonrelativistic value ω_cn:

$$\omega_\mathrm{c} = \frac{\omega_\mathrm{cn}}{\gamma_\mathrm{rel}} = \omega_\mathrm{cn}\left(1 - \frac{1}{2}\beta^2\right) + \mathcal{O}(\beta^4).$$

The relativistic factor is $\gamma_\mathrm{rel} = (1-\beta^2)^{-1/2}$ in terms of β, the total electron velocity normalized to c. Since the axial velocity of electrons is constant and the field profile is assumed fixed, the derivative of the transversal momentum with respect to time can be replaced by the derivative with respect to the axial coordinate z.

Finally, it is convenient to introduce the following dimensionless variables:

$$\zeta = \frac{C_1\omega}{c}z \qquad \tau = \frac{1}{2}C_1^2\omega t \qquad \xi = \frac{1}{2}C_1^2 m\varphi$$
$$p = \frac{\tilde{P}}{|\tilde{P}_0|} \qquad f = \frac{C_2 e J_{m+1}(\kappa R_{\mathrm{el}})}{|\tilde{P}_0|}F \qquad \Delta = C_2(\omega - \omega_{\mathrm{c}0}), \tag{2.10}$$

where $C_1 = \beta_{\perp 0}^2/2\beta_{\parallel 0}$, $C_2 = 2/\omega\beta_{\perp 0}^2$, $\beta_\perp$ and $\beta_\parallel$ are the transversal and axial velocities normalized to c, m is the azimuthal index of the mode, and the subscript '0' refers to the values at the entrance into the cavity. Together with the Taylor expansion for ω_{c}, these normalizations bring equation (2.9) into the final dimensionless form

$$\frac{\mathrm{d}p}{\mathrm{d}\zeta} + \mathrm{i}(\Delta + |p|^2 - 1)p = \mathrm{i}f(\zeta, \xi, \tau). \tag{2.11}$$

In the most general case, the field envelope f is allowed to depend on the azimuthal coordinate ξ and time τ in addition to the axial coordinate ζ. These dependences are explicitly indicated in parentheses.

2.2.4 Wave equation for the high-frequency field

The derivation of the time-dependent equation for the RF field under the influence of the electron beam has been published in reference 69. It is assumed that the transversal structure of the field is fixed (a TE mode) so that only the axial profile is free to evolve in time. Here, the derivation of this model is described and the generalization into two spatial dimensions is briefly discussed thereafter.

Combining Maxwell's equations for the curl of electric and magnetic fields, we obtain

$$-\nabla\times(\nabla\times\mathbf{E}) - \frac{1}{c^2}\frac{\partial^2\mathbf{E}}{\partial t^2} = \mu_0\frac{\partial\mathbf{j}}{\partial t}.$$

With the help of the identity $\nabla\times(\nabla\times\mathbf{E}) = \nabla(\nabla\cdot\mathbf{E}) - \nabla^2\mathbf{E}$, this can be transformed into a wave equation. Simple estimates based on typical gyrotron beam parameters show that the charge density gradient term $\nabla(\nabla\cdot\mathbf{E}) = \nabla\rho/\epsilon_0$ can be neglected in comparison to $\nabla^2\mathbf{E}$. As a result, we obtain the wave equation for electromagnetic waves in the presence of an electric current:

$$\nabla^2\mathbf{E} - \frac{1}{c^2}\frac{\partial^2\mathbf{E}}{\partial t^2} = \mu_0\frac{\partial\mathbf{j}}{\partial t}. \tag{2.12}$$

Let us separate the dependences of the electric field on different coordinates as in equation (2.5) and assume the current density to have the same harmonic time dependence as the electric field. Furthermore, let us assume slow variation of the field amplitude, $|\partial F/\partial t| \ll \omega|F|$, use the Helmholtz equation (2.6), which determines the transversal structure of the field, and perform the following manipulations: First, equation (2.12) [with (2.5) substituted for $\mathbf{E}$] is multiplied with $\mathbf{E}_{\mathrm{t}}^*$ and integrated over the waveguide cross-section $S_\perp$. Then, the result is multiplied with $\exp(-\mathrm{i}\omega t)$ and finally averaged over the microwave oscillation period $2\pi/\omega$. As a result, an equation obtained for the evolution of $F(z,t)$:

$$\frac{\partial^2 F}{\partial z^2} + \frac{\omega^2 - \omega(z)^2}{c^2}F - 2\mathrm{i}\frac{\omega}{c^2}\frac{\partial F}{\partial t} = \frac{\mathrm{i}\omega\mu_0}{N}\int_{S_\perp}\mathbf{j}_\omega\cdot\mathbf{E}_{\mathrm{t}}^*\,\mathrm{d}S_\perp, \tag{2.13}$$

where

$$N = \int_{S_\perp} \mathbf{E}_\mathrm{t} \cdot \mathbf{E}_\mathrm{t}^* \, \mathrm{d}S_\perp \quad \text{and} \quad \mathbf{j}_\omega = \frac{1}{2\pi} \int_0^{2\pi} \mathbf{j} \mathrm{e}^{-\mathrm{i}\omega t} \, \mathrm{d}(\omega t)$$

are the norm of the wave and the Fourier component of the beam current density, respectively.

The integrals above can be readily evaluated by substituting the solution (2.7) for the electric field $\mathbf{E}_t$ and noting that net current arises from the bunching of electrons, which are all located at the radial position $r = R_\mathrm{el}$. The resulting expressions suggest that a suitable definition for a dimensionless beam current is [81]

$$I = \frac{4e}{\pi \epsilon_0 m_\mathrm{e} c^3} \frac{\beta_{\parallel 0} I_0}{\beta_{\perp 0}^6} \frac{J_{m\pm1}^2 \left(2\pi R_\mathrm{el}/\lambda\right)}{\gamma_\mathrm{rel}(\nu^2 - m^2) J_m^2(\nu)}, \tag{2.14}$$

where I_0 is the beam current, λ is the wavelength, and ν is a zero of the derivative of J'_m (corresponding to the specific mode TE_{mp}). For modes co-rotating with the electrons, the function J_{m-1} is used in equation (2.14), and for counter-rotating modes J_{m+1}. Usually the electron beam radius is adjusted to coincide with the first maximum of $J_{m\pm1}$ to achieve strongest possible interaction. The slow longitudinal variation of $\omega(z)$ is described by the dimensionless function

$$\delta(z) = \frac{2}{C_1^2 \omega} \left[\omega - \omega(z)\right]. \tag{2.15}$$

With this notation, we obtain the dimensionless form of equation (2.13):

$$\frac{\partial^2 f}{\partial \zeta^2} - \mathrm{i}\frac{\partial f}{\partial \tau} + \delta f = \frac{I}{2\pi} \int_0^{2\pi} p \, \mathrm{d}\vartheta_0. \tag{2.16}$$

The current term on the right-hand side is computed as an averaged momentum of the beam electrons, which obey their equation of motion given in the previous section. The initial gyrophases of electrons are denoted by ϑ_0.

Following references 75 and 76, the dependence of f on the azimuthal coordinate can be taken into account in equation (2.16). Here, the electric field is assumed to have the form $\mathbf{E} \sim f \exp[\mathrm{i}(\omega t - m\varphi)]$ and the field envelope to depend only weakly on the spatial coordinates: $|\partial f/\partial \zeta| \ll |f|/\lambda$ and $|\partial f/\partial \varphi| \ll m|f|$. Also the fact that the beam radius is close to the caustic of the TE_{mp} wave is taken into account. The equation governing the evolution of f in the resulting spatio-temporal formalism is

$$\frac{\partial^2 f}{\partial \zeta^2} - \mathrm{i}\frac{\partial f}{\partial \xi} - \mathrm{i}\frac{\partial f}{\partial \tau} + \delta f = \frac{I}{2\pi} \int_0^{2\pi} p \, \mathrm{d}\vartheta_0. \tag{2.17}$$

In a cylindrical resonator in which the cut-off frequency along the axis equals identically the cut-off frequency at the exit, $\omega(z) \equiv \omega$, and consequently, $\delta \equiv 0$, the last term on the left-hand side can be dropped out. Throughout this thesis, this idealization has been used. The only exception is section II-B of publication 4, which discusses how artificial reflections could be introduced with the help of the function $\delta(\zeta)$.

2.2.5 Initial and boundary conditions

At the entrance cross-section, the electrons are evenly distributed over different gyrophases and have equal energies. The initial condition for equation (2.11) governing their momenta can thus be written as

$$p(0) = \mathrm{e}^{\mathrm{i}\vartheta_0} \quad \text{with} \quad 0 \le \vartheta_0 < 2\pi. \tag{2.18}$$

The partial differential equation (2.17) requires boundary conditions in ζ and ξ as well as an initial condition. The boundary condition for f at the entrance cross section states that the waves can not propagate into the input taper, and the field should therefore vanish:

$$f(0, \xi, \tau) = 0. \tag{2.19}$$

At the exit ($\zeta = \zeta_{\text{out}}$), a non-reflecting boundary is assumed:

$$\left[f(\zeta, \xi, \tau) + \frac{1}{\sqrt{\mathrm{i}\pi}} \int_0^\tau \frac{1}{\sqrt{\tau - \tau'}} \frac{\partial f(\zeta, \xi, \tau')}{\partial \zeta} \, \mathrm{d}\tau' \right]_{\zeta=\zeta_{\text{out}}} = 0, \tag{2.20}$$

which is essentially obtained by a Fourier transform from simple radiation boundary conditions for all frequency components of the RF field [69]. In the azimuthal direction, the field must have the periodicity of 2π in φ, so that

$$f(\zeta, \xi + \xi_{\max}, \tau) = f(\zeta, \xi, \tau) \quad \text{for all } \xi, \tag{2.21}$$

where $\xi_{\max} = C_1^2 m\pi$ [see equations (2.10)]. Finally, the initial condition used in the computations of this work is

$$f(\zeta, \xi, 0) = \left[0.1 + 0.01 \sin\left(\frac{2\pi\xi}{\xi_{\max}} \right) \right] \sin\left(\frac{\pi\zeta}{\zeta_{\text{out}}} \right), \tag{2.22}$$

which models a field profile with one maximum in the axial direction and a small azimuthal perturbation due to nonzero amplitudes of the neighboring modes.

2.3 Numerical algorithms

2.3.1 Discretization of the gyrotron equations

The advances in computation technology allow using more straightforward methods for solving equations (2.11) and (2.17) than in the 1980's [69, 76]. When the transverse structure of the RF field is assumed fixed, the problem is one-dimensional. In reference 69, the solution was found using a rather complicated numerical method based on Laplace transformations. In this thesis, the equations were discretized, which converts the partial differential equation into a tridiagonal linear system easily solved at each time step with standard numerical algorithms. While the two methods give completely equivalent results in the one-dimensional approximation, the situation is somewhat different when the full two-dimensional form of equations (2.11) and (2.17) is considered. In reference 76, the method of characteristics was used. The integration of the equations was carried out along characteristic curves, which are diagonal with respect to the coordinate axes. Thus, it is rather difficult to interpret the results, even though the essential physical phenomena (loss of stability, efficiency fluctuations) can be perfectly detected. Instead, by generalizing the discretization scheme into two spatial dimensions, the equations can be efficiently solved using a sparse matrix library routine, giving the results in a very transparent form. The generalized two-dimensional scheme is described below; the one-dimensional version can be obtained as the special case $K = 1$, *i.e.*, by reducing the number of grid points in the azimuthal direction to one.

The domain of interest in the (ζ, ξ, τ) space is discretized with step sizes $\Delta\zeta$, $\Delta\xi$, and $\Delta\tau$, and the value of f at a grid point is denoted as

$$f(j\Delta\zeta, k\Delta\xi, n\Delta\tau) \equiv f^n_{j,k},$$

where $j = 0, 1, \ldots, J$; $k = 0, 1, \ldots, K-1$; and $n = 0, 1, \ldots$. Using this notation, the derivatives in equations (2.11) and (2.17) can be replaced by the approximations

$$\frac{\partial^2 f}{\partial \zeta^2} \quad \longrightarrow \quad \frac{f^{n+1}_{j+1,k} - 2f^{n+1}_{j,k} + f^{n+1}_{j-1,k}}{(\Delta\zeta)^2} \tag{2.23}$$

$$\frac{\partial f}{\partial \tau} \quad \longrightarrow \quad \frac{f^{n+1}_{j,k} - f^{n}_{j,k}}{\Delta\tau} \tag{2.24}$$

$$\frac{\partial f}{\partial \xi} \quad \longrightarrow \quad \frac{f^{n+1}_{j,k+1} - f^{n+1}_{j,k-1}}{2\Delta\xi}. \tag{2.25}$$

This discretization scheme is fully implicit (f^{n+1} and not f^n in the spatial derivatives) and centered in both spatial dimensions. (Strictly speaking, the reflectionless boundary condition at $\zeta = \zeta_{\text{out}}$ can not be treated implicitly.) Implicit schemes generally have much better numerical properties than explicit schemes, and this is particularly true for diffusion-like problems [89]. The current term is replaced by

$$g^n_{j,k} \equiv \frac{I}{s} \sum_{l=1}^{s} p(j\Delta\zeta, k\Delta\xi, n\Delta\tau, \vartheta_0^{(l)}), \tag{2.26}$$

defined as the net transverse momentum of the electrons in an s-particle ensemble with different initial gyrophases. As far as the boundary condition (2.20) is concerned, it is possible to isolate the singularity in the integrand if the function $\partial f/\partial\zeta$ satisfies the first-order Lipschitz condition [90] with some constant L

$$\left| \frac{\partial f}{\partial \zeta} - \left[\frac{\partial f}{\partial \zeta} \right]_{\zeta=\zeta_{\text{out}}} \right| < L|\zeta - \zeta_{\text{out}}|.$$

As a result, one obtains a difference approximation also for equation (2.20):

$$f^n_{J,k} + \sqrt{\frac{\Delta\tau}{\mathrm{i}\pi}} \left(2\sqrt{n} \frac{f^n_{J,k} - f^n_{J-1,k}}{\Delta\zeta} + \sum_{\nu=0}^{n-1} \frac{f^\nu_{J,k} - f^\nu_{J-1,k} - f^n_{J,k} + f^n_{J-1,k}}{\Delta\zeta\sqrt{(n-\nu)}} \right) = 0 \tag{2.27}$$

for $k = 0, 1, ..., K-1$. The discrete problem can now be written in matrix form:

$$A^n \mathbf{f}^{n+1} = \mathbf{c}^n, \tag{2.28}$$

where

$$\mathbf{f}^n = \begin{pmatrix} f^n_{0,0} & \cdots & f^n_{0,K-1} & f^n_{1,0} & \cdots & f^n_{J,K-1} \end{pmatrix}^{\mathrm{T}}$$

and

$$\mathbf{c}^n = \begin{pmatrix} c^n_{0,0} & \cdots & c^n_{0,K-1} & c^n_{1,0} & \cdots & c^n_{J,K-1} \end{pmatrix}^{\mathrm{T}}.$$

The coefficient matrix has a block tridiagonal form:

$$A^n = \begin{pmatrix} I & & & & \\ a_1 I & B & a_1 I & & \\ & \ddots & \ddots & \ddots & \\ & & a_1 I & B & a_1 I \\ & & & a^n_2 I & a^n_3 I \end{pmatrix}, \quad \text{where} \quad B = \begin{pmatrix} b_1 & -b_2 & & & b_2 \\ b_2 & b_1 & -b_2 & & \\ & \ddots & \ddots & \ddots & \\ & & b_2 & b_1 & -b_2 \\ -b_2 & & & b_2 & b_1 \end{pmatrix},$$

and I is the $K \times K$ identity matrix. B is a cyclic tridiagonal matrix due to the periodic boundary condition in ξ, and the expressions for its elements as well as for a_1, a_2, a_3^n, and $c_{j,k}^n$ can be found in publication 6. For a typical choice $J = K = 60$, the linear system (2.28) has 3660 unknowns and the coefficient matrix A^n about 10^7 elements, only about 10^4 of which are nonzero. It is evident that sparse matrix techniques are suitable for this problem. The IMSL library routine DLSLZG, which solves a complex sparse system of linear equations by Gaussian elimination [91] was successfully applied.

To obtain the discrete current term (2.26), equation (2.11) is solved by a standard Runge-Kutta algorithm using the already known field $f(\zeta, \xi, \tau)$.

2.3.2 Accuracy and stability

Rounding errors unavoidably occur during numerical computations. It is of central importance to prevent accumulation of these errors in the course of computations consisting of billions of elementary operations. Two principal questions to be considered separately when selecting a numerical method are its *accuracy* and *stability*.

A good numerical method utilizes maximally the capability of the computer to represent numbers in binary form. For example, if the two operands of a binary operation have been expressed as 16-bit binary numbers, all effort should be made to have 16 significant bits in the result of the operation as well. A simple example of an operation where this is not possible (bad accuracy) is the subtraction of two almost equal numbers. In such a case most of the significant bits are equal and there are only a few different low-order bits in the binary representations of the numbers. In subtraction, the equal bits are lost; effectively the result is expressed with a much worse precision than the machine would allow. Usually, such operations can be circumvented by algebraic manipulations of the expressions containing the dangerous operations. The philosophy in this thesis has been to use existing numerical routines [89, 91] when available to minimize the risk of operations with bad accuracy.

Another aspect of numerical accuracy is the ability of an approximate method to reproduce the exact mathematical answer. There are often several alternative methods for a particular task. Typically, advanced methods reach the same level of accuracy with fewer steps than primitive ones, thus being more efficient in use—although often considerably more complicated to implement. In this thesis commonly used, rather elementary schemes have been sufficiently fast, even when the step sizes have been chosen conservatively to gain better accuracy. The spatial step sizes fulfill the stability criteria for a discretized parabolic partial differential equation. It was also checked that a decrease in the step size does not bring any new features into the numerical solution. In particular, the excitation of competing modes in 2D computations was observed independently of the azimuthal step size when the mode number exceeded a critical value.

The integration of the equation of motion for electrons is the most straightforward numerical task of this thesis. The fourth-order Runge-Kutta scheme has been successfully used with a step size $\Delta\zeta = 0.25$. Here, a comparative solution was computed in publication 1 with different software and a much smaller step size, showing excellent agreement. For example, careful comparison of figure 3.4 to figures 9 and 10 of publication 1 shows that the energy spectrum is very similar in both cases; the peak positions differ only about 0.3 degrees.

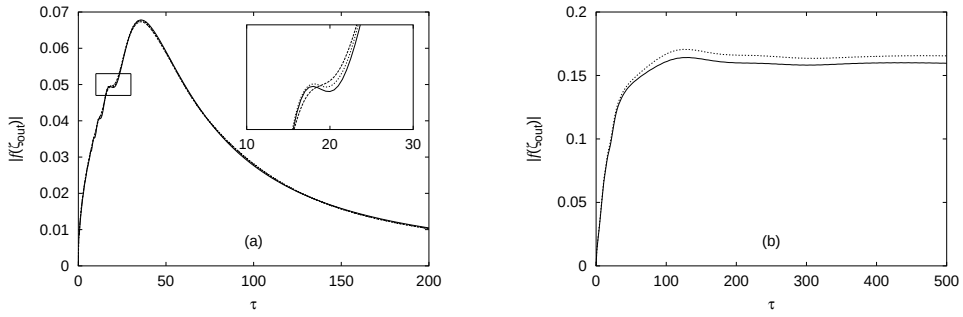

FIGURE 2.1. *(a) Analytic solution (2.30) with $a = 0.1$ and $\zeta_{\text{out}} = 15$ (solid line) and corresponding numerical solutions from the 1D model for $\Delta\tau = 0.1$ (dashed) and $\Delta\tau = 0.02$ (dotted). Inset: a blowup of the region of rapid changes. (b) The solutions of equations (2.16) and (2.17) computed with the 1D (solid line) and 2D (dotted) codes, respectively. The operating parameters are $\Delta = 0.6$ and $I = 0.01$.*

The one-dimensional field equation (2.16) is a parabolic partial differential equation, resembling the diffusion equation. The fully implicit discretization scheme for the diffusion equation is stable for arbitrarily large time steps [89]. The spatial step size $\Delta\zeta = 0.25$ was again found to be sufficiently small. For the time step, the value $\Delta\tau = 0.02$ was used in the solution of the one-dimensional problem, providing excellent resolution still keeping the computation times short. The accuracy of the results can be assessed by comparing the numerical and analytic solutions for a special case. In reference 68, an integral representation for equation (2.16) was found with the help of Laplace transformation:

$$f(\zeta,\tau) = \frac{1}{2}\sqrt{\frac{\mathrm{i}}{\pi}}\int_0^{\zeta_{\text{out}}} f(x,0)G(x,\zeta,\tau)\,\mathrm{d}x - \frac{1}{\sqrt{2\mathrm{i}\pi}}\int_0^{\zeta_{\text{out}}}\int_0^{\tau} B(x,\tau-\tau')G(x,\zeta,\tau')\,\mathrm{d}\tau'\,\mathrm{d}x, \tag{2.29}$$

where $B(\zeta,\tau)$ is the right-hand side of equation (2.16), and the Green function for a semi-infinite regular ($\delta \equiv 0$) waveguide is given by the expression

$$G(x,\zeta,\tau) = \frac{1}{\sqrt{\tau}}\left\{\exp\left[-\mathrm{i}\frac{(x-\zeta)^2}{4\tau}\right] - \exp\left[-\mathrm{i}\frac{(x+\zeta)^2}{4\tau}\right]\right\}.$$

With $I = 0$ and the initial condition $f(\zeta,0) = a\sin(\pi\zeta/\zeta_{\text{out}})$, an analytic expression can be written for the field amplitude at $\zeta = \zeta_{\text{out}}$:

$$f(\zeta_{\text{out}},\tau) = -\frac{\mathrm{i}a}{4}\exp\left[\frac{\mathrm{i}\pi^2\tau}{\zeta_{\text{out}}^2}\right] \times\left\{2\,\mathrm{erf}\left[\frac{\pi\sqrt{\mathrm{i}\tau}}{\zeta_{\text{out}}}\right] - \mathrm{erf}\left[\sqrt{\frac{\mathrm{i}}{\tau}}\left(\frac{\pi\tau}{\zeta_{\text{out}}} - \zeta_{\text{out}}\right)\right] - \mathrm{erf}\left[\sqrt{\frac{\mathrm{i}}{\tau}}\left(\frac{\pi\tau}{\zeta_{\text{out}}} + \zeta_{\text{out}}\right)\right]\right\}. \tag{2.30}$$

This is plotted with numerical solutions for $\Delta\tau = 0.1$ and $\Delta\tau = 0.02$ in figure 2.1(a).

Successful integration in one spatial dimension provided reference cases for the two-dimensional computations. In that case the number of elementary operations is much larger, and the time step was increased to 0.1 to speed up the computation. Whenever the solutions remained azimuthally symmetric, good agreement with the ones obtained in one-dimensional computations was found [see figure 2.1(b)].

CHAPTER 3

Results

3.1 Electron trajectories

3.1.1 Cold-cavity approximation

We start with the approximations which can be made in the equations (2.11) and (2.17), when electron trajectories are investigated: First, a stationary field ($\partial f/\partial\tau = 0$) is assumed. Next, the dependence on the azimuthal coordinate can be neglected ($\partial f/\partial\xi = 0$). Finally, one can make the so-called cold-cavity approximation assuming that the high-frequency field profile does not depend on the electron beam current, but is determined solely by the geometry of the cavity. This decouples the equations and allows one to solve them separately. As a result, we obtain the simplest equation which describes the electron motion in a gyrotron resonator [79]:

$$\frac{\mathrm{d}p}{\mathrm{d}\zeta} + \mathrm{i}(\Delta + |p|^2 - 1)p = \mathrm{i}f(\zeta)F \tag{3.1}$$

with the initial condition $p(\zeta_0) = \exp(\mathrm{i}\vartheta_0)$, where $0 \leq \vartheta_0 < 2\pi$. Here, the dimensionless electron beam to RF coupling factor F has been introduced, since the absolute magnitude of the RF field f cannot be determined from (2.17) in the cold-cavity approximation. The expression for F can be found, *e.g.*, in reference 92. Correspondingly, the equation for the cold-cavity field profile becomes

$$\frac{\mathrm{d}^2 f}{\mathrm{d}\zeta^2} + \gamma^2 f = 0, \tag{3.2}$$

where the function $\gamma = \delta^{1/2}$ depends on the frequency of oscillations, on the quality factor, and on the geometry of the resonator.

The orbital efficiency $\eta_\perp$ of a gyrotron is the portion of transverse energy which is extracted from the beam during the interaction. It can be calculated by averaging electron momenta at the resonator exit cross section $\zeta = \zeta_{\mathrm{out}}$ over the initial phase:

$$\eta_\perp = 1 - \frac{1}{2\pi}\int_0^{2\pi} |p(\zeta_{\mathrm{out}})|^2 \,\mathrm{d}\vartheta_0.$$

3.1.2 Hamiltonian approach

In publication 1, the Hamiltonian approach was used for mathematical classification of electron trajectories. Assuming that in an idealized resonator the real and imaginary part of $f(\zeta)$ can be represented as periodic functions, it was found that there are two elliptic and one hyperbolic fixed point and that no chaotic solutions exist. Figure 3.1 shows an example of the Poincaré map.

In realistic resonators, the cold-cavity RF field can be approximated by a Gaussian distribution

$$f(\zeta) = \exp\left[-\left(\frac{2\zeta}{\mu} - \sqrt{3}\right)^2\right], \tag{3.3}$$

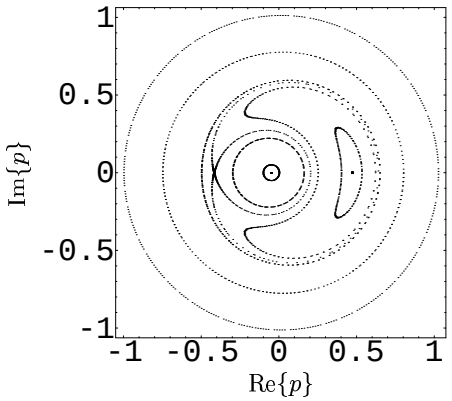

FIGURE 3.1. *Poincaré map of electrons in an infinitely long resonator. Elliptic fixed points are located at* $(-0.05, 0)$ *and* $(0.47, 0)$ *and a hyperbolic fixed point at* $(-0.42, 0)$*. Here* $\Delta = -0.20$ *and* $F = 0.01$*. [P1]*

where μ is the dimensionless length of the resonator. This approximation is valid in resonators with high quality factors. In a specific resonator $f(\zeta)$ is found by solving the second-order differential equation (3.2) with the boundary conditions

$$\left[\frac{\mathrm{d}f}{\mathrm{d}\zeta} - \mathrm{i}\gamma(\zeta)f\right]_{\zeta=0} = 0, \qquad \left[\frac{\mathrm{d}f}{\mathrm{d}\zeta} + \mathrm{i}\gamma(\zeta)f\right]_{\zeta=\zeta_{\mathrm{out}}} = 0.$$

Figure 3.2 shows a typical example of $f(\zeta)$.

The finding of reference 66 that the motion of electrons in the vicinity of some particular initial angles is very sensitive to the exact value of the initial angle was confirmed in publication 1 (see figure 3.3). Moreover, some self-similarity was discovered (figure 3.4), which supports the hypothesis that electron trajectories not only diverge on different sides of a separatrix but become truly chaotic.

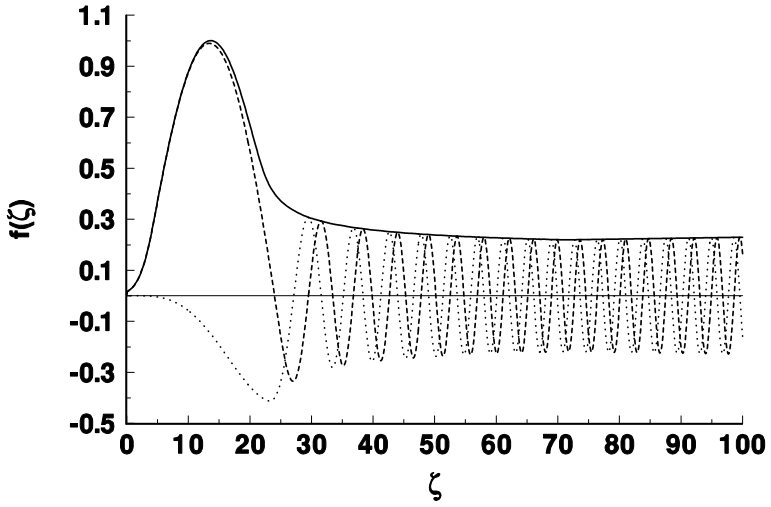

FIGURE 3.2. *The longitudinal profile of the* RF *field in a realistic gyrotron resonator corresponding to* $\mu \approx 9$*. The curves show the modulus of* f *(solid line), the real part of* f *(dashed), and the imaginary part of* f *(dotted). [P1]*

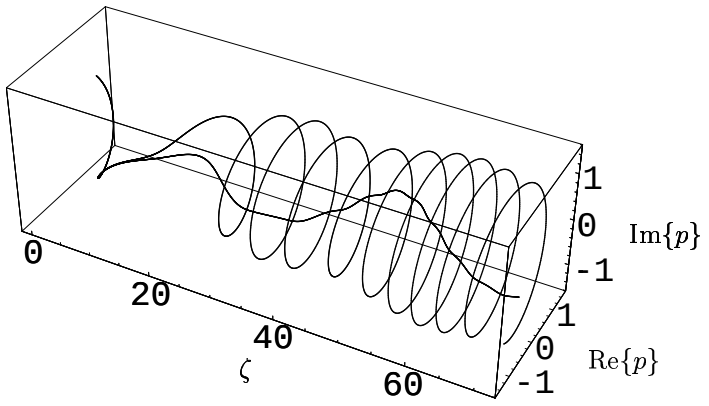

FIGURE 3.3. *Three-dimensional trajectories of two electrons with close initial conditions: 33.4 and 33.9 degrees. The two trajectories begin at $p \approx 0.832 + 0.554\,\mathrm{i}$ and diverge at $p \approx -0.6 + 0.25\,\mathrm{i}$. The resonator is the same as in figure 3.2, and the parameters are $\Delta = 0.5$, $F = 0.125$. [P1]*

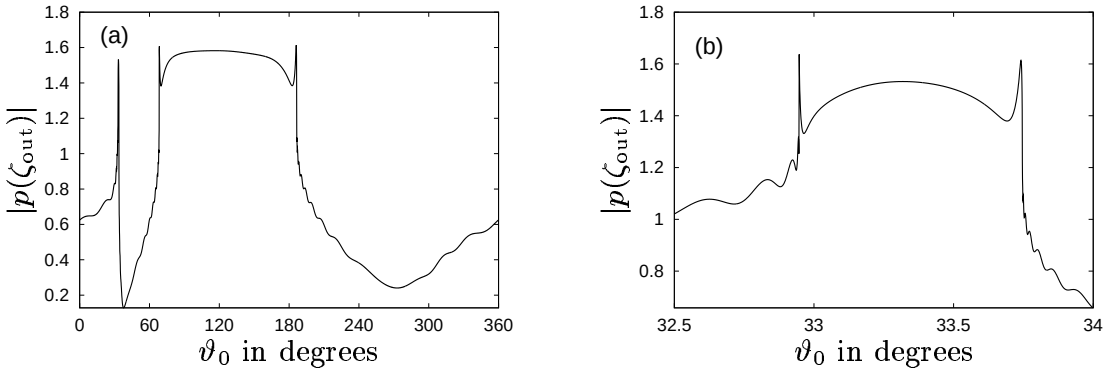

FIGURE 3.4. *(a) Transverse momentum of electrons at the resonator end as a function of the initial angle. (b) The same, but in an enlarged section around the first peak. The parameters are the same as in figure 3.3, and the orbital efficiency is $\eta_\perp = 0.06$. [P1]*

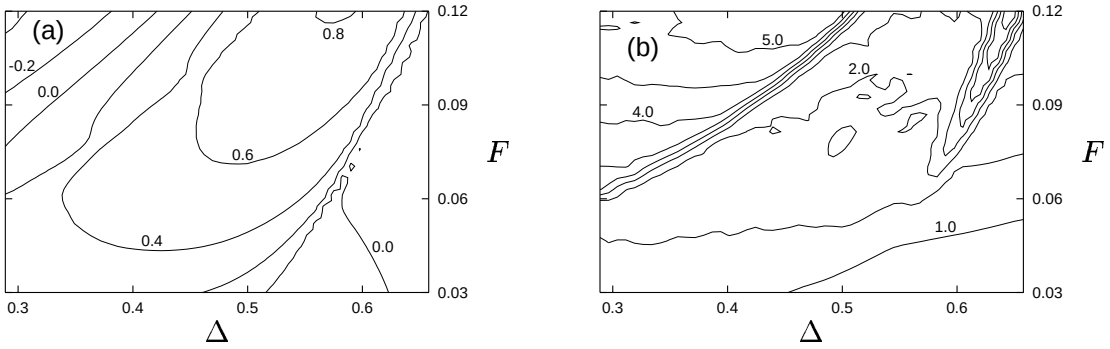

FIGURE 3.5. *(a) Contours of $\eta_\perp$ and (b) contours of S in the plane of generalized gyrotron parameters Δ and F. The calculation was done for a specific resonator with $\mu = 12.8$. [P1]*

3.1.3 Application to depressed collectors

Chaos-like behavior of electron trajectories allows one to conclude that there are electrons whose energy cannot be predicted after they leave the interaction space. The larger the current, the larger is the number of such electrons. To quantify the degree of complexity of the residual energy spectrum of electrons, the quantity

$$S = \int_0^{2\pi} \left| \frac{\mathrm{d}|p(\zeta_{\mathrm{out}})|}{\mathrm{d}\vartheta_0} \right| \mathrm{d}\vartheta_0, \tag{3.4}$$

called the *smoothness* (should more appropriately be called *complexity*) of the spectrum, was defined in publication 1. Large values of S indicate that sensitive dependence on initial conditions is seen at many initial angles. Although the connection between chaos and this functional is, in fact, weak, it still serves well together with the orbital efficiency $\eta_\perp$ to distinguish between three different regimes of interaction, which can be seen in figures 3.5(a)–(b). Figure 3.6 shows one residual energy spectrum corresponding to each regime. In the central region of figure 3.5, the efficiency is high and the spectrum is mostly regular. Around the upper left corner the interaction becomes too strong (*overbunching*), and on the right-hand edge the interaction is too weak for the extraction of the energy from the electron beam. There are even regimes with $\eta_\perp < 0$, in which electrons would on average gain energy from the electromagnetic field instead of transferring it to the field. In real gyrotrons without any external injection of RF energy into the cavity, there would be absolutely no oscillations in these regions.

From the results presented in figures 3.5 and 3.6, it can be concluded that chaos in electron residual energies is virtually absent in the region where a gyrotron is operated with high efficiency. One can estimate the maximum applicable collector potential, which is limited by the requirement that many electrons must not be reflected by the retarding electric field. In publication 2, an expression was derived for the critical value $p_{\text{cut-off}}$ of the output momentum, which only just suffices to bring an electron to the collector:

$$|p(\zeta_{\mathrm{out}})| > p_{\text{cut-off}} \equiv \frac{1}{\alpha\sqrt{1-b}} \sqrt{\frac{2\phi_{\mathrm{coll}} + \phi_{\mathrm{coll}}^2}{2\phi_{\mathrm{cath}} + \phi_{\mathrm{cath}}^2}(1+\alpha^2) - 1}. \tag{3.5}$$

Here $b = B_{\mathrm{coll}}/B_{\mathrm{cav}}$ is the magnetic decompression factor between the collector and

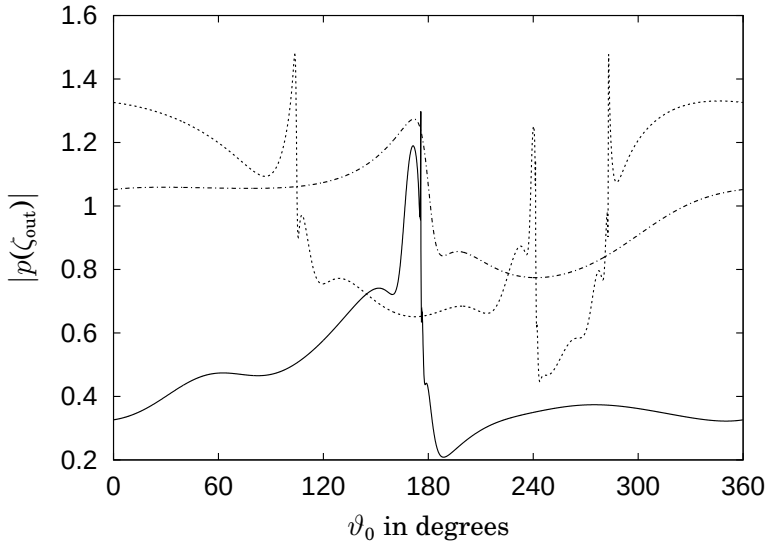

FIGURE 3.6. *Three residual momentum spectra. $\Delta = 0.55$, $F = 0.11$, $\eta_\perp = 0.78$, $S = 2.1$ (solid line); $\Delta = 0.60$, $F = 0.05$, $\eta_\perp \approx 0$, $S = 1.0$ (dash-dot); $\Delta = 0.35$, $F = 0.10$, $\eta_\perp \approx 0$, $S = 4.6$ (dotted). [P1]*

the cavity, $\phi_{\rm coll}$ and $\phi_{\rm cath}$ are the collector and cathode voltages normalized to $m_{\rm e}c^2/e$, and α is the pitch factor of the incoming beam. The right-hand side is called $p_{\text{cut-off}}$ since all electrons with $|p(\zeta_{\rm out})| < p_{\text{cut-off}}$ are "cut off" from the spectrum by reflection. In reference 93 this was applied to the calculation of electron efficiencies of specific gyrotrons. Figure 3.7 shows how the achieved efficiency increase is lost as the electrons begin to be trapped. Here, adiabatic reflection refers to the extreme case in which the retardation length $\Delta z_{\rm ret}$ of an electron in the electric field of the depressed collector is large in comparison to its spatial Larmor period $\Delta z_{\rm L}$. Conversely, reflection is said to be non-adiabatic when $\Delta z_{\rm ret} \ll \Delta z_{\rm L}$.

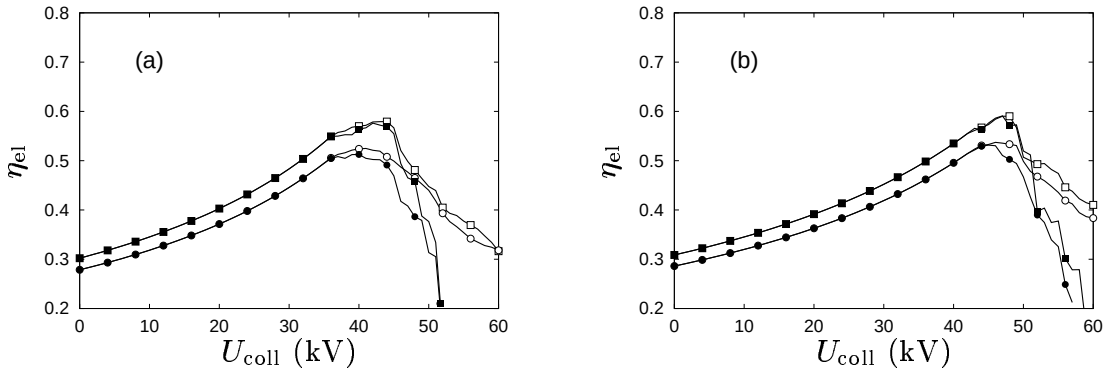

FIGURE 3.7. *The calculated electron efficiency of two gyrotrons as a function of the collector potential depression. Adiabatic reflection, no velocity spread (filled squares); adiabatic reflection, 10 % velocity spread (filled circles); non-adiabatic reflection, no velocity spread (open squares); non-adiabatic reflection, 10 % velocity spread (open circles). (a) The 1 MW, 140 GHz conventional gyrotron for W7-X [48]. (b) The 2.2 MW, 165 GHz coaxial cavity gyrotron at the Forschungszentrum Karlsruhe [94]. The electron efficiency $\eta_{\rm el} = \eta_\perp \alpha^2/(1+\alpha^2)$. [93]*

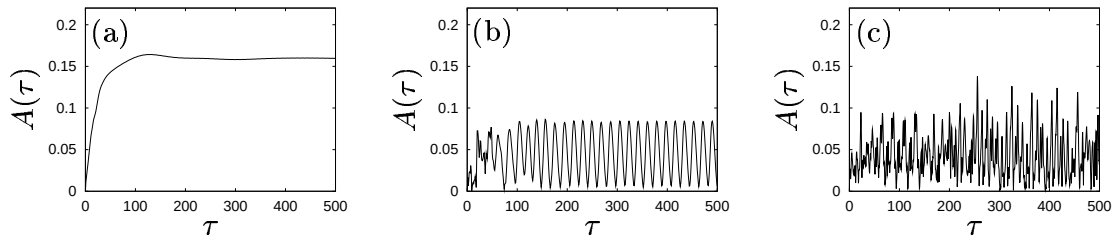

FIGURE 3.8. *The field amplitude $A(\tau) \equiv |f(\zeta_{\text{out}}, \tau)|$ at the resonator end as a function of time. (a) Stationary signal for $\Delta = 0.60$, $I = 0.01$. (b) Automodulation for $\Delta = -0.05$, $I = 0.15$. (c) Chaos for $\Delta = -0.30$, $I = 0.15$. [P3]*

3.2 Chaotic RF oscillations

3.2.1 Ideal case

Time-dependent behavior determined by the system of equations (2.11) and (2.16) has been investigated in references 68 and 69, where stationary oscillations were found to become periodically modulated and chaotic as the beam current increases. Figure 3.8 illustrates the different kinds of solutions. In publication 3, this theory was reconsidered and a new method was presented for straightforward numerical solution of the equations. That work also reports the calculation of a map of gyrotron oscillation regimes, which shows that the regions of stationary oscillations, automodulation and chaos have a complicated topology in the plane of generalized gyrotron variables Δ and I (see figure 3.9). The resonator was assumed to be cylindrical ($\delta \equiv 0$) with dimensionless length $\mu = 15$, and the generated wave was let to propagate freely out of the cavity. The reflectionless boundary condition (2.20) was used at the resonator output cross-section to fulfill this requirement.

In reference 95 it was studied whether any of the classical routes to chaos (period doubling, quasi-periodicity, intermittency or the transient route) is relevant for gyrotrons. This was done by plotting the local minima and maxima of $A(\tau) \equiv |f(\zeta_{\text{out}}, \tau)|$ in time along lines $\Delta = -0.30$ and $I = 0.20$ in the parameter plane. The resulting diagrams are shown in figure 3.10. In (a), one can see traces of period doubling, while (b) shows traces of intermittency.

3.2.2 Effect of velocity spread and reflections

The effect of velocity spread of electrons was studied in publication 3. In general, the inclusion of the spread changes the results very little. The solutions become qualitatively different only in the vicinity of boundaries of the regions shown in figure 3.9. This demonstrates that figure 3.9 can be used to roughly estimate the behavior of a gyrotron even in the presence of a 20 % velocity spread.

Reflections of microwaves from the window, the load, or transmission line inhomogeneities can significantly lower the threshold for nonstationary oscillations and open possibilities for utilization of chaos for specific purposes [71, 96]. Reflections influence also mode competition in gyrotrons [97, P5], and recently it has been suggested that they can lead to complicated quasiperiodic patterns of the signal instead of chaos [73, 74, 98]. These studies were extended in publication 4, where a new description of reflections was introduced: reflection is taken into account by artifi-

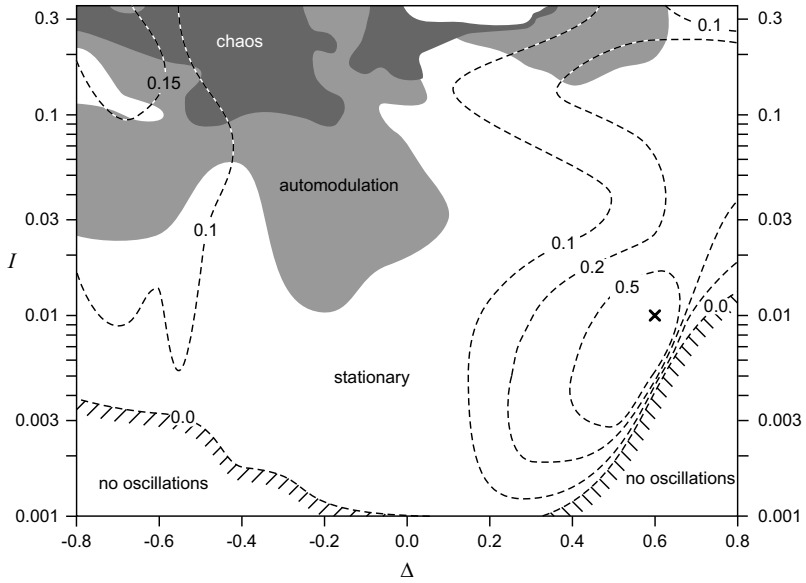

FIGURE 3.9. *Topology of different kinds of oscillations of a gyrotron in the* (Δ, I) *plane. White regions correspond to stationary oscillations, gray regions correspond to automodulation, and dark regions to chaotic oscillations. The contours of constant efficiency are shown by dashed lines. The point of the maximum efficiency* $\eta_{\perp}^{\max}$*= 0.75 is marked by the cross. Here* $\mu = 15$*. [P3]*

cially launching a backward-traveling wave representing the delayed reflected signal. Compared to previous studies of nonstationary oscillations with allowance for reflections, this approach is rather general by nature, since it has been worked out with the simplest model for the resonator—cylindrical—without any assumptions about the cause of reflection. The reflection is described by the reflection coefficient R and the delay time T. Some results of this study are given in figures 3.11 and 3.12, showing in the presence of reflection an output signal with its power spectrum and the "map" of different oscillation regimes, respectively. Figure 3.11 addresses the question whether reflections drive the system into chaos and not into a quasiperiodic orbit. The signal appears to be aperiodic, but its spectrum reveals that it is to a large extent composed of a few frequencies. This is the most typical case in the parameter region of interest, and therefore the conclusion made in [73] can be confirmed: usually reflection leads to quasiperiodicity instead of chaos.

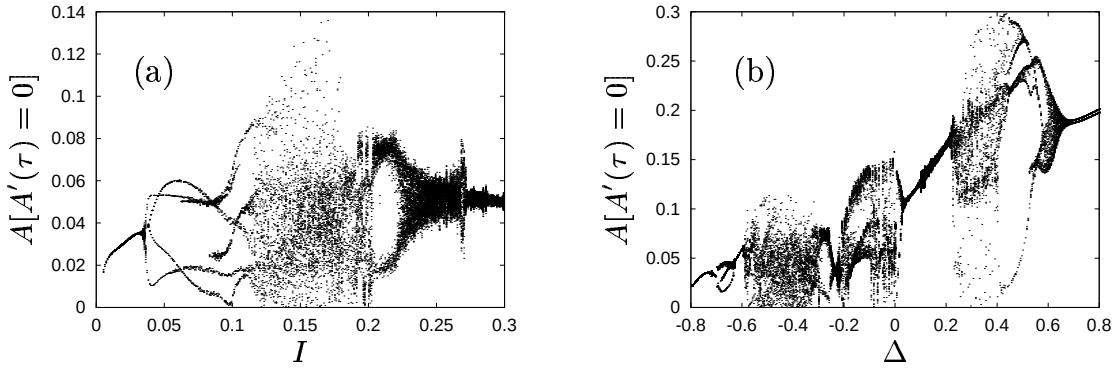

FIGURE 3.10. *Routes to chaos. (a) Along the line* $\Delta = -0.30$ *in figure 3.9, traces of period doubling are seen. (b) Along the line* $I = 0.20$*, traces of intermittency appear. [95]*

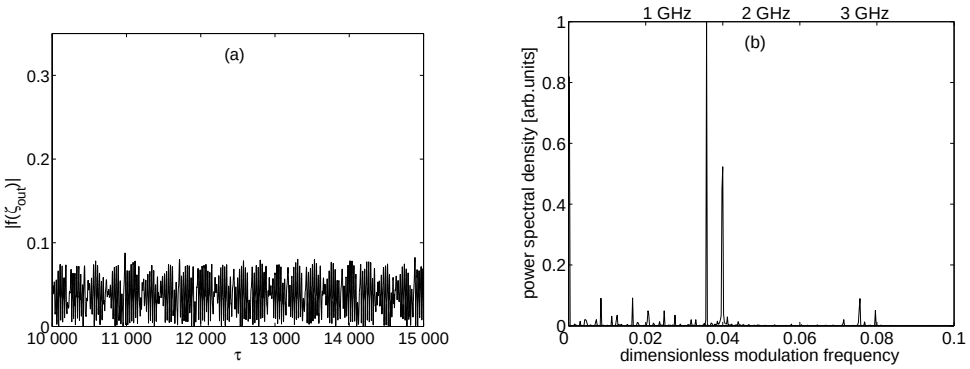

FIGURE 3.11. *(a) A quasiperiodic gyrotron signal. (b) The power spectrum of the signal. Here $\Delta = 0.0$, $I = 0.017$, amplitude reflection coefficient $R = 0.45$, and dimensionless reflection delay time $T = 200$. [P4]*

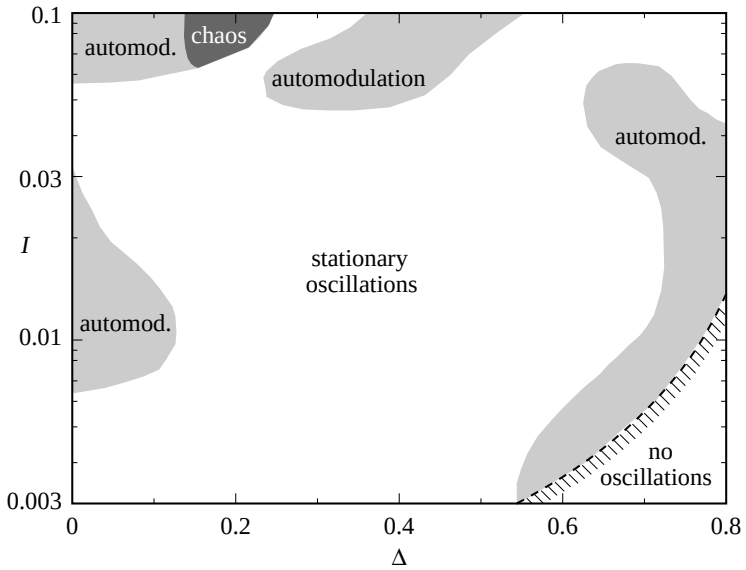

FIGURE 3.12. *Topology of different kinds of oscillations of a gyrotron in the (Δ, I) plane with reflection coefficient $R = 0.45$ and dimensionless delay $T = 200$. The white region corresponds to stationary oscillations, gray regions correspond to automodulation, and the dark region to chaotic oscillations. Compare to figure 3.9 but note that the parameter ranges differ. [P4]*

3.2.3 Feasibility of experimental confirmation of the results

Estimations show [P3] that high-power, high-frequency gyrotrons, as for example the 2.2 MW, 165 GHz coaxial cavity gyrotron developed at the Forschungszentrum Karlsruhe [94], cannot be used to generate automodulated or chaotic oscillations, since they operate at low values of the dimensionless current ($I \approx 0.003$). The predictions shown in figure 3.9 could be easily checked in gyrotrons operating in low-order modes, because for such modes, the same value of the electron beam current corresponds to a significantly larger dimensionless current. Some confirmation for the results comes from observations of automodulation in a relativistic gyrotron [99] and possibly chaotic oscillations of a gyrotron with a high-current explosive electron emission cathode [100]. Also, complicated nonstationary phenomena with alternating stationary and chaotic zones have recently been found in a gyro-BWO [101].

3.3 Spatio-temporal chaos

3.3.1 Ideal case

If the diameter of a resonator is much larger than the wavelength, as is the case in high-frequency high-power gyrotrons, many resonator modes may fall within the cyclotron resonance band. Then it is meaningful to go over from a single-mode representation of the RF field to a spatio-temporal description, in which the envelope of the RF field is a continuous function of the transversal coordinates [76]. In this case, the system of equations (2.11) and (2.17) has to be solved without any simplifications. This was done in publication 6 by extending the numerical method presented in publication 3 to the case of two spatial variables. It was found that there exist critical values of m, the azimuthal index of mode, beyond which gyrotron oscillations become nonstationary and azimuthally asymmetric. These values m_{crit} were calculated for particular values of Δ and I (figure 3.13). For small values of the dimensionless current I and $m > m_{\mathrm{crit}}$, the favorable operating mode is suppressed by competing modes with a different axial structure and lower efficiency. Mode competition manifests itself as wild oscillations of the field envelope (see figure 3.14).

For high beam current ($I \approx 0.1$) we can expect chaotic spatio-temporal behavior of the field envelope f owing to the excitation of several competing modes. Such results were obtained in publication 6, but their validity was challenged by the pre-examiner [102] of this thesis. Indeed, the numerical solution was found to depend on the grid size and time steps used. Therefore, it is most probable that figure 3 of that article represents *numerical chaos* instead of a real effect and does not yet provide tenable evidence for the existence of spatio-temporal chaos in this system.

There are several papers [103–105] devoted to studying numerical chaos in the nonlinear Schrödinger equation, and maybe also the linear equation (2.17) can show numerical chaos because of the coupling into the nonlinear equation (2.11). The emergence of numerical chaos can be avoided with a proper choice of the discretization scheme. Alternative discretizations to that given in equations (2.23)—(2.25) should be studied to facilitate proper numerical treatment of the high-current cases as well. The results shown in figures 3.13 and 3.14 were found to be numerically more stable; nonetheless, it is appropriate to relax the estimated error in m_{crit} from ± 2 to about ± 5 everywhere in figure 3.13.

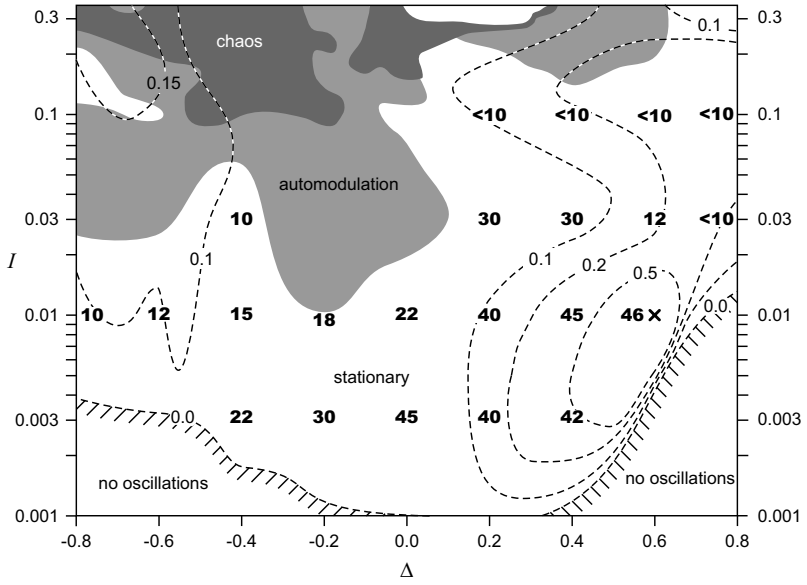

FIGURE 3.13. *The upper limit for m (numbers in boldface) for stationary gyrotron oscillations in the (Δ, I) plane. The background regimes and efficiency contours are taken from figure 3.9. Here $\mu = 15$. [P6]*

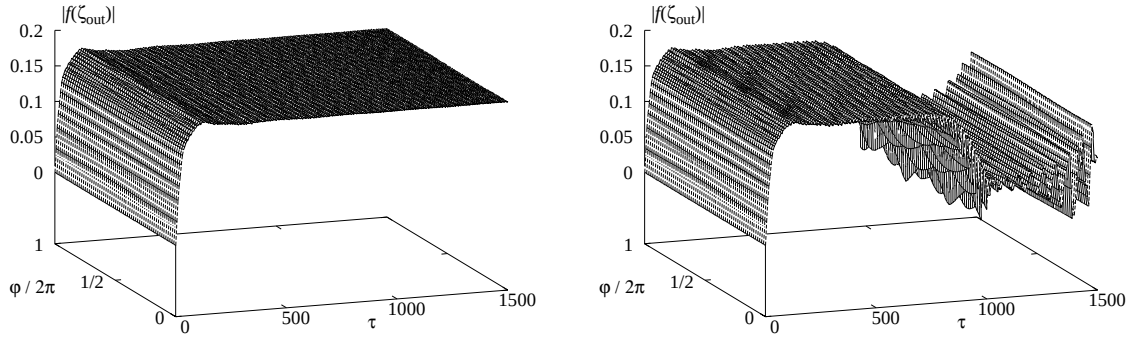

FIGURE 3.14. *The amplitude of the high-frequency field at the output cross section as a function of azimuthal angle φ and dimensionless time τ for $m = 45$ and $m = 50$, respectively. Here $\Delta = 0.60$ and $I = 0.01$. [P6]*

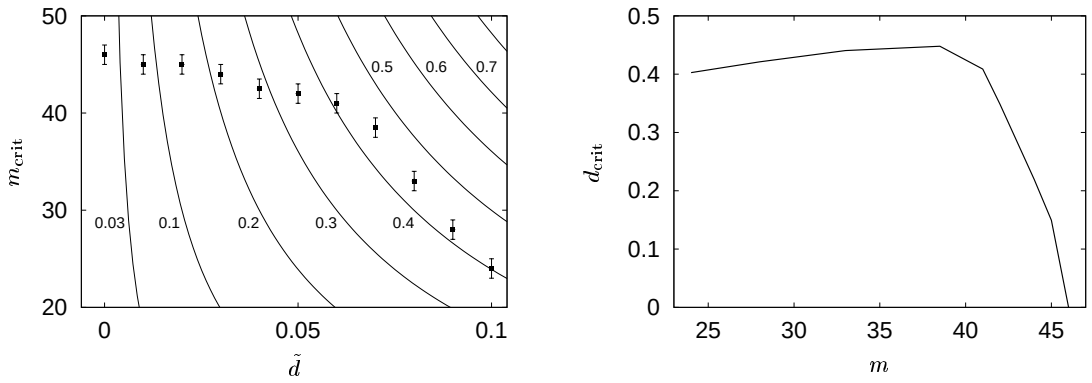

FIGURE 3.15. *(a) Critical azimuthal index of the mode as a function of* $\tilde{d} = D/R_{\mathrm{el}}$ *(filled squares). Also the contours of* $d = D/\lambda$ *are shown. The error bars indicate how precisely* m_{crit} *could be estimated with reasonable computational cost. (b) Maximum tolerable beam displacement* $d = D/\lambda$ *as a function of the azimuthal index of the mode. Here* D *is the displacement,* R_{el} *the beam radius,* λ *the wavelength, and the operating parameter values are* $\Delta = 0.60$, $I = 0.01$. *[P7]*

It should be emphasized that the critical values of m strongly depend on the cavity length. For example, for $\mu = 10$ the maximum efficiency is obtained with $\Delta = 0.73$, $I = 0.038$, and at this point $m_{\mathrm{crit}} = 29$. For $\mu = 20$, these numbers are $\Delta = 0.52$, $I = 0.0039$, and $65 < m_{\mathrm{crit}} < 70$. Evidently, stationary single-mode oscillations can be sustained as long as diffraction effects do not become too strong. The significance of diffraction can be related to the so called Fresnel parameter $C_{\mathrm{F}} = L^2/[8R\lambda(1 - m^2/\nu^2)^{1/2}]$, where L and R are the resonator length and radius respectively, λ is the wavelength, and ν is the eigenvalue of the mode [106]. In terms of the dimensionless gyrotron variables, this parameter can be written as $C_{\mathrm{F}} = \beta_{\|0}^2\mu^2/[4\pi\beta_{\perp 0}^4(\nu^2 - m^2)^{1/2}]$, $\beta_{\|0}$ and $\beta_{\perp 0}$ being the normalized axial and transverse velocities of the electron beam, respectively. In real tubes, typical values of the Fresnel parameter are between 0.5 and 1.5.

3.3.2 Effect of electron beam misalignment

In practice, several factors may make the electron beam deviate transversally from its desired position in the cavity. The shorter the wavelength, the more sensitive the tube is to beam misalignment. In publication 7, the results obtained in publication 6 have been generalized by relaxing the requirement of a concentrically placed beam. The variation of the critical value of the azimuthal index of the mode m is shown as a function of $\tilde{d} = D/R_{\mathrm{el}}$ in figure 3.15(a). While these data points serve well to extend the investigations of the ideal case [P6] in terms of the formalism presented in publication 7, the same data are shown again in a more application-related way in figure 3.15(b). Instead of $\tilde{d}$ one is often more interested in the quantity $d = D/\lambda$, whose contours are shown in figure 3.15(a). Figure 3.15(b) was obtained by plotting the maximum tolerable value d_{crit} of d as a function of m. This example has been calculated with $\Delta = 0.60$, $I = 0.01$, which is the point of maximum efficiency. The value $m_{\mathrm{crit}} = 46$ reflects the fact that d_{crit} goes to zero at $m = 46$.

CHAPTER 4

Summary and discussion

4.1 Electron trajectories

In publication 1, electron trajectories in an idealized gyrotron resonator—infinitely long and with an idealized force in the form of trigonometric functions—were classified using the Hamiltonian method. It was proved that in this case the system is fully integrable and that no chaotic motions appear. This indirectly confirms the results of reference 65 where no chaotic behavior of electron trajectories was found assuming a traveling plane wave. In real (finite) gyrotron resonators with a realistic strong, aperiodic force, the motion of electrons in the vicinity of some particular initial phases is very sensitive to the exact value of the initial phase. This sensitivity suggests that the trajectories of the electrons for these particular initial conditions may become chaotic. The larger the current, the larger is the number of such electrons. Calculating the perpendicular efficiency and smoothness of the electron residual energy spectrum for a specific value of μ = 12.8 and varying Δ and F, it was found that the regions of high efficiency in general coincide with the regions of good smoothness.

Publication 2 reports the development of a formalism, which describes electrostatic trapping of electrons due to a depressed collector and takes it into account in gyrotron efficiency calculations. The two opposite extreme cases of perfectly adiabatic and very non-adiabatic reflection were considered. Several representative sets of generalized gyrotron parameters were chosen as examples. In addition, the theory was applied to two specific gyrotrons to find the optimum voltage of the depressed collector. It is evident from figures 2 and 3 of publication 2 that the trapping effect is more probable and pronounced in the operating regimes with high perpendicular efficiency. Indeed, here many electrons have very low residual energies at the exit from the cavity. They make largest contributions to efficiency. At the same time, these "good" electrons have the strongest tendency to become trapped. For example, at the point of the highest efficiency (μ = 17, F = 0.125) with U_{coll} = 33 kV, some of the "best" electrons traverse the cavity six times before they acquire from the RF field the energy which is needed for leaving the trap. It is also seen (figures 5 and 8 of publication 2) that just for these μ and F values the increase of the efficiency due to the retarding potential as $U_{\mathrm{cath}}/(U_{\mathrm{cath}} - U_{\mathrm{coll}})$ breaks down already at $U_{\mathrm{coll}} \approx 30$ kV because of the onset of trapping, while in two other cases trapping begins at higher collector voltages. Generally, the velocity spread tends to smooth the transition to the trapping region. In gyrotrons whose cavities have a low quality factor, the dependences shown in figures 4–6 of publication 2 should be observed, while in the case of high quality factors, weaker dependence on the velocity spread, such as shown in figures 7–9 of publication 2, should be expected.

The calculations indicate that one could use retarding potentials as high as 35–40 kV in the 1 MW, 140 GHz gyrotron [figure 3.7(a)] and 40–45 kV in the 2.2 MW, 165 GHz coaxial gyrotron [figure 3.7(b)] without efficiency decrease due to electron trapping. The difference between the cases of the adiabatic and non-adiabatic reflection manifests itself only at very high collector voltages. In the adiabatic case, the

efficiency decrease is much more drastic. Non-adiabatically reflected electrons do not re-enter the cavity to disturb RF generation, and at very high retarding potentials the efficiency levels out at the same value as it is without a depressed collector.

The calculated maximal collector voltages are higher than those used in experiments [94, 107]; in both gyrotrons, efficiency begins to decrease when the collector voltage exceeds 33 kV. There are several factors which have been neglected in this thesis but could explain the observation: First, the conversion of the transversal momentum to axial motion is incomplete due to the finite decompression and possibly a steep gradient of the magnetic field. Second, backscattering of primary or secondary electrons may occur even when electrons have enough parallel momentum to reach the collector. Finally, in practice neither the adiabatic nor the non-adiabatic approximation describes the real reflection, which is something between these extreme cases. Therefore, if reflected or backscattered electrons return to the cavity, their pitch factor can have any value, which was not accounted for in the calculations.

4.2 Nonstationary oscillations

The onset of chaotic oscillations in gyrotrons was reconsidered in publication 3. A simple and straightforward numerical method for solving the system of underlying partial differential equations was used. It was found that the topology of the domains of different kinds of oscillations is more complicated than envisaged earlier. In particular, alternating sequences of regions of stationary, automodulation, and chaotic oscillations were found in the plane of the generalized gyrotron variables: frequency mismatch and dimensionless current. There is a large margin for increasing the output power by raising the current without a risk of excitation of chaotic oscillations.

An estimate can be given for the bifurcation current for automodulation or chaos in realistic devices. As an example, consider the 2.2 MW, 165 GHz coaxial cavity gyrotron developed at the Forschungszentrum Karlsruhe [94]. This gyrotron operates in the $\mathrm{TE}_{31,17}$ mode with a gun that delivers 84 A current and whose pitch factor at 90 kV is 1.3. Equation (2.14) thus gives $I = 0.003$, and the normalized interaction length of an 18 mm cavity is $\mu = 17$. On one hand, this value of I shows that there is a large margin to raise the output power of the gyrotron by raising the current. On the other hand, it is clear that this gyrotron cannot be used to test the predictions shown in figures 3.8(b)–(c). For this purpose, one would need to increase the current of the gun up to about 5000 A, which is not realistic. As is evident from equation (2.14), the dimensionless current is inversely proportional to $\alpha\beta_{\perp 0}^5$, where $\alpha = \beta_{\perp 0}/\beta_{\parallel 0}$. It is interesting to note that during the startup of this gyrotron, the working mode $\mathrm{TE}_{31,17}$ passes through the automodulation region ($\Delta = -0.25$ and $I = 0.042$ at 60 kV; $\Delta = 0.01$ and $I = 0.027$ at 65 kV) before reaching the operating point $\Delta = 0.47$ and $I = 0.003$ at 90 kV. Because of mode competition, these automodulation oscillations probably cannot be observed, since they will be suppressed by competing modes, which have much more favorable values of Δ and I [94]. Such oscillations could be observed in special experiments, in which the magnetic compression and thus the electron orbital velocity in the cavity would be decreased leading to a large increase of I. It should be easier to check the predictions shown in figure 3.9 in gyrotrons operating in low-order modes, because for such modes the dimensionless current is much larger for comparable values of the gun current.

In some special applications (material processing, special-purpose radars), chaotic oscillations are desirable. From figure 3.9 it is obvious that under normal circumstances (reasonable currents, high efficiency, high power) chaotic oscillations cannot be generated. However, it has been suggested that artificially introduced reflections could significantly decrease bifurcation currents for chaos (see, *e.g.*, reference 71). In the present theory, such reflections can be modeled by the function $\delta(\zeta)$, as was done in reference 97. Unfortunately, this method is not quite suitable for investigating reflections taking place at a distance much larger than the cavity length. In this thesis, a more flexible formulation to describe reflections in the self-consistent time-dependent gyrotron theory was developed, and the numerical algorithm needed for the corresponding computations was given. The most important parameters characterizing reflection were concluded to be the absolute value of the reflection coefficient and the delay time. When stationary oscillations are considered, the reflection phase could be used instead of the delay time. The effect of the reflection phase on the stationary field profile and, consequently, on the generation efficiency is rather strong. Using a three-wave description, reflections from distant objects can be simulated without remarkably slowing down the computations. However, the system itself attains its final state in a time scale that is much longer than the delay, so the computer runs unavoidably become longer than in the idealized case.

It was found that new regions of nonstationary oscillations are generated and the existing ones shift to slightly lower currents owing to reflection. The results support the idea that reflection tends to drive a gyrotron into quasiperiodic (as suggested in reference 73) rather than chaotic oscillations (as claimed in reference 71). Chaos appears in figure 3.12 just as a curiosity indicating small changes in the locations of the chaotic regimes in the parameter space. It is interesting that automodulation was found for almost all current values when $0.6 \leq \Delta \leq 0.8$. This is in sharp contrast with the reflectionless case where the high-efficiency region is surrounded by regimes of stationary oscillations only. The findings can therefore be exploited in the development of high-power gyrotrons, which should provide a stationary signal even in the case of accidental reflections. By identifying in the operating parameter plane those regions, where chaotic oscillations may be obtained, the results also ease the design of gyrotrons for applications, which require broad bandwidth.

Influence of reflections on the operation of the coaxial cavity gyrotron for Iter was investigated using the self-consistent theory of mode competition. It was found that the gyrotron is sufficiently robust against possible frequency-independent reflections of RF power, and that the amount of reflected power should not exceed 1 %. Also, the designed diamond window turned out to assure single-mode operation of the gyrotron in the desired $\mathrm{TE}_{34,19}$ mode, although it was assumed that the window be placed just at the exit of the cavity. This assumption can be regarded as a worst-case scenario; in reality, the effect of reflections will necessarily be significantly weaker, since not all reflected power will return into the cavity through the mode converter.

4.3 High-order mode operation

As far as operation at high values of the azimuthal index m is concerned, it was shown that there exist maximal values m_{crit}, beyond which stationary single-mode operation of a gyrotron is no longer possible. Surprisingly, these critical numbers are

rather low ($m_{\text{crit}} \lesssim 46$) for high-power gyrotrons with typical operation parameters α = 1.35 and U = 92 kV (compare with reference 76) even in the region of highest efficiencies. This limits the attempts to minimize Ohmic losses by going over to large-diameter cavities and to high-order whispering gallery operating modes. This also means that one should have $m \lesssim 23$ for a gyrotron operating both in the fundamental and second harmonic. In reference to previous work, the calculated value $m_{\text{crit}} \approx 46$ for Δ = 0.6 and I = 0.01 can be compared to that (about 44) obtained with a different method [76].

A straightforward way to include electron beam misalignment into the self-consistent two-dimensional model for time-dependent gyrotron oscillations was presented. Since heavy computations were required, the study focused on two combinations of the generalized gyrotron parameters, Δ and I. Both for positive and negative Δ, increasing misalignment tends to lower the threshold above which stationary single-mode operation becomes impossible. This is the effect one would expect symmetry-breaking to have. There also exists an opposite effect: the effective beam current decreases when the beam is shifted [see equation (7) of publication 7], and more regular behavior is generally seen at lower currents. The results suggest, however, that symmetry breaking dominates in the cases studied here. From the practical point of view, the most significant result of the beam misalignment calculations is shown in figure 3.15(b). As was shown in publication 6, the ultimate limit for high-efficiency operation is at $m \approx 46$. In publication 7, it became evident that in the region $40 \lesssim m \lesssim 46$ the operating mode is very sensitive to beam misalignment. For example, the critical misplacement d_{crit} is about 0.15 for m = 45, which means 0.26 mm in a 170 GHz gyrotron. Together with high-order mode operation, one should therefore always consider how precisely the beam can be placed into its correct position in the resonator. Once the wavelength and operating mode have been specified, figure 3.15(b) can be used for a rough estimate of the tolerance in beam position. To compare with other effects of beam misalignment, figure 3.15(a) is useful. The slight decline of m_{crit} with increasing $\tilde{d}$ is accompanied by much more severe changes in efficiency and starting current. For example, when $\tilde{d}$ = 0.06, m_{crit} is still about 40, but perpendicular efficiency has dropped by 32 % from its ideal value, and the starting current correspondingly increased by 47 % (see references 108, 109).

4.4 Controlling chaos in gyrotrons

Controlling chaos has not yet been studied in gyrotrons. For example, one could imagine to control chaos by stabilizing an unstable periodic orbit by making only small but rapid time-dependent perturbations on an available system parameter [110]. In the case of gyrotrons, in the regions where only temporal chaos occurs, one would wish to stabilize a particular shape of $|f(\zeta)|$, *e.g.*, that with only one maximum, which provides high gyrotron efficiency. This could be done by making only small time-dependent adjustments on control parameters Δ and I. It is interesting to note that in lasers this method of controlling chaos has been demonstrated experimentally (see, for example, reference 111).

Bibliography

[1] World Population Prospects Population Database: The 2002 Revision. United Nations Population Division. Retrieved from http://esa.un.org/unpp/ on January 15, 2004.

[2] J. Ongena and G. Van Oost, *Energy for future centuries. Will fusion be an inexhaustible, safe and clean energy source?*, Trans. Fusion Sci. Technol. **41**, 3 (2002).

[3] Energy Needs, Choices and Possibilities. Scenarios to 2050. Shell International (2001).

[4] Kyoto Protocol to the United Nations Framework Convention on Climate Change. Retrieved from http://unfccc.int/resource/docs/convkp/conveng.pdf on January 15, 2004.

[5] Key World Energy Statistics 2003 from the IEA. The International Energy Agency. Retrieved from http://www.iea.org/statist/ on January 15, 2004.

[6] L. A. Artsimovich, S. V. Mirnov and V. S. Strelkov, *Investigation of the Ohmic heating of a plasma in the 'Tokamak-3' toroidal apparatus*, Plasma Phys. (J. Nucl. Energy Part C) **7**, 305 (1965). Translated from Атомная Энергия **17**, 170 (1964).

[7] L. A. Artsimovich *et al.*, *Экспериментальные исследования на установках Токамак (Experiments in Tokamak devices)*, Plasma Phys. Controll. Nucl. Fusion Res. **1**, 157 (1969). In Russian.

[8] A. Iiyoshi *et al.*, *Overview of the Large Helical Device project*, Nucl. Fusion **39**, 1245 (1999).

[9] Large Helical Device web site at http://www.lhd.nifs.ac.jp/ (January 15, 2004).

[10] M. Wanner *et al.*, *Design and construction of WENDELSTEIN 7-X*, Fusion Eng. Des. **56–57**, 155 (2001).

[11] Wendelstein 7-X web site at http://www.ipp.mpg.de/eng/for/projekte/w7x/ (January 15, 2004).

[12] K. A. Brueckner (editor), *Inertial Confinement Fusion* (American Institute of Physics, New York, 1992).

[13] *Energy from Inertial Fusion* (International Atomic Energy Agency, Vienna, 1995).

[14] National Ignition Facility web site at http://www.llnl.gov/nif/ (January 15, 2004).

[15] J. Wesson, *Tokamaks* (Oxford University Press, New York, 1997), second edition.

[16] EFDA-JET web site at http://www.jet.efda.org/ (January 15, 2004).

[17] M. Keilhacker *et al.*, *High fusion performance from deuterium-tritium plasmas in JET*, Nucl. Fusion **39**, 209 (1999).

[18] M. Yoshikawa, *An overview of the JT-60 project*, Fusion Eng. Des. **5**, 3 (1987).

[19] JT-60 web site at http://www-jt60.naka.jaeri.go.jp/ (January 15, 2004).

[20] J. L. Luxon and L. G. Davis, *Big Dee—A flexible facility operating near breakeven conditions*, Fusion Tech. **8**, 441 (1985).

[21] DIII-D web site at http://fusion.gat.com/diii-d/ (January 15, 2004).

[22] W. Köppendörfer, *ASDEX Upgrade – ein Tokamakexperiment mit reaktorrelevantem Divertor (ASDEX Upgrade. A tokamak experiment with a reactor-relevant divertor)*, Phys. Bl. **46**, 324 (1990). In German.

[23] ASDEX Upgrade web site at http://www.ipp.mpg.de/eng/for/projekte/asdex/ (January 15, 2004).

[24] B. Turck, *TORE SUPRA: A tokamak with superconducting toroidal field coils. Status report after the first plasmas*, IEEE Trans. Mag. **25**, 1473 (1989).

[25] TORE SUPRA web site at http://www-drfc.cea.fr/cea/ts/ts.htm (January 15, 2004).

[26] Iter web site at http://www.iter.org/ (January 15, 2004).

[27] Y. Shimomura *et al.*, *ITER-FEAT operation*, Nucl. Fusion **41**, 309 (2001).

[28] A. Ando *et al.*, *Plasma current generation and sustainment by electron cyclotron waves in the WT-2 tokamak*, Phys. Rev. Lett. **56**, 2810 (1986).

[29] H. Tanaka *et al.*, *Non-inductive current drive using second harmonic electron cyclotron waves on the WT-3 tokamak*, Nucl. Fusion **31**, 1673 (1991).

[30] V. V. Alikaev *et al.*, *Electron cyclotron current drive experiments on T-10*, Nucl. Fusion **32**, 1811 (1992).

[31] O. Sauter *et al.*, *Steady-state fully noninductive current driven by electron cyclotron waves in a magnetically confined plasma*, Phys. Rev. Lett. **84**, 3322 (2000).

[32] N. A. Kirneva, *Recent developments in electron cyclotron current drive*, Plasma Phys. Controll. Fusion **43**, A195 (2001).

[33] G. Dammertz, private communication (2003).

[34] A. V. Gaponov-Grekhov (editor), *Гиротрон. Сборник научных трудов (Gyrotron. Collected Papers)* (Institute of Applied Physics, Academy of Sciences of the USSR, Gorky, 1981). In Russian.

[35] V. A. Flyagin (editor), *Гиротроны. Сборник научных трудов (Gyrotrons. Collected Papers)* (Institute of Applied Physics, Academy of Sciences of the USSR, Gorky, 1989). In Russian.

[36] C. J. Edgcombe (editor), *Gyrotron Oscillators—Their Principles and Practice* (Taylor & Francis, London, 1993).

[37] A. V. Gaponov-Grekhov and V. L. Granatstein (editors), *Applications of High-Power Microwaves* (Artech House, Boston, 1994).

[38] R. A. Cairns and A. D. R. Phelps (editors), *Generation and Application of High Power Microwaves* (Institute of Physics Publishing, Bristol, 1996).

[39] R. J. Barker and E. Schamiloglu (editors), *High-Power Microwave Sources and Technologies*, IEEE Press Series on RF and Microwave Technology (John Wiley & Sons, IEEE Press, New York, 2001), first edition.

[40] J. Schneider, *Stimulated emission of radiation by relativistic electrons in a magnetic field*, Phys. Rev. Lett. **2**, 504 (1959).

[41] R. H. Pantell, *Backward-wave oscillations in an unloaded waveguide*, Proc. IRE **47**, 1146 (1959).

[42] A. V. Gaponov, *Взаимодействие непрямолинейных электронных потоков с электромагнитными волнами в линиях передачи (Interaction of irrectilinear electron beams with electromagnetic waves in transmission lines)*, Изв. Высш. Учебн. Завед. Радиофиз. **2**, 450 (1959). English translation in Radiophys. Quantum Electron.

[43] I. B. Bott, *A powerful source of millimetre wavelength electromagnetic radiation*, Phys. Lett. **14**, 293 (1965).

[44] T. V. Borodacheva, A. L. Goldenberg and V. N. Manuilov, *О рекуперации в гиротроне (On energy recovery in a gyrotron)*, in *Гиротроны. Сборник научных трудов (Gyrotrons. Collected Papers)* (edited by V. A. Flyagin), pp. 161–180 (Institute of Applied Physics, Academy of Sciences of the USSR, Gorky, 1989). In Russian.

[45] M. E. Read, W. G. Lawson, A. J. Dudas and A. Singh, *Depressed collectors for high-power gyrotrons*, IEEE Trans. Electron Dev. **37**, 1579 (1990).

[46] K. Sakamoto *et al.*, *Major improvement of gyrotron efficiency with beam energy recovery*, Phys. Rev. Lett. **73**, 3532 (1994).

[47] R. Heidinger, G. Dammertz, A. Meier and M. K. Thumm, *CVD diamond windows studied with low- and high-power millimeter waves*, IEEE Trans. Plasma Sci. **30**, 800 (2002).

[48] G. Dammertz *et al.*, *Development of a 140-GHz 1-MW continuous wave gyrotron for the W7-X stellarator*, IEEE Trans. Plasma Sci. **30**, 808 (2002).

[49] G. Dammertz *et al.*, *Progress of the 1 MW, 140 GHz, CW gyrotron for W7-X*, in *Conf. Digest, 27th Int. Conf. on Infrared and Millimeter Waves* (edited by R. J. Temkin), pp. 3–4, IEEE (IEEE Press, Piscataway, 2002).

[50] Technical Basis for the ITER Final Design, ITER EDA Documentation Series No. 24. IAEA (2001).

[51] B. Piosczyk *et al.*, *A 1.5-MW, 140-GHz, $TE_{28,16}$ coaxial cavity gyrotron*, IEEE Trans. Plasma Sci. **25**, 460 (1997).

[52] B. Piosczyk *et al.*, *Coaxial cavity gyrotron with dual RF beam output*, IEEE Trans. Plasma Sci. **26**, 393 (1998).

[53] B. Piosczyk *et al.*, *165 GHz, 1.5 MW-coaxial cavity gyrotron with depressed collector*, IEEE Trans. Plasma Sci. **27**, 484 (1999).

[54] B. Piosczyk *et al.*, *Step-frequency operation of a coaxial cavity gyrotron from 134 to 169.5 GHz*, IEEE Trans. Plasma Sci. **28**, 918 (2000).

[55] B. Piosczyk *et al.*, *Coaxial cavity gyrotron—Recent experimental results*, IEEE Trans. Plasma Sci. **30**, 819 (2002).

[56] B. Piosczyk *et al.*, *Towards a 2 MW, CW, 170 GHz coaxial cavity gyrotron for ITER*, in *Book of Abstracts, 22nd Symp. on Fusion Technology* (edited by S. Tähtinen, R. Rintamaa, M. Asikainen and H. Tuomisto), p. 180, Association Euratom-Tekes (Otamedia Oy, Espoo, 2002).

[57] B. Piosczyk *et al.*, *Experimental results and technical requirements for a 2 MW, CW, 170 GHz coaxial cavity gyrotron*, in *Conf. Digest, 27th Int. Conf. on Infrared and Millimeter Waves* (edited by R. J. Temkin), pp. 7–8, IEEE (IEEE Press, Piscataway, 2002).

[58] E. Borie *et al.*, *Possibilities for multifrequency operation of a gyrotron at FZK*, IEEE Trans. Plasma Sci. **30**, 828 (2002).

[59] O. Dumbrajs, J. A. Heikkinen and H. Zohm, *Electron cyclotron heating and current drive control by means of frequency step tunable gyrotrons*, Nucl. Fusion **41**, 927 (2001).

[60] Yu. V. Bykov *et al.*, *Селекция мод в мощных гиротронах (Mode selection in powerful gyrotrons)*, in *Гиротрон. Сборник научных трудов (Gyrotron. Collected Papers)* (edited by A. Gaponov-Grekhov), pp. 185–191 (Institute of Applied Physics, Academy of Sciences of the USSR, Gorky, 1981). In Russian.

[61] B. G. Danly, K. E. Kreischer, W. J. Mulligan and R. J. Temkin, *Whispering-gallery-mode gyrotron operation with a quasi-optical antenna*, IEEE Trans. Plasma Sci. **13**, 383 (1985).

[62] K. E. Kreischer and R. J. Temkin, *Single-mode operation of a high-power, step-tunable gyrotron*, Phys. Rev. Lett. **59**, 547 (1987).

[63] E. Ott, *Chaos in Dynamical Systems* (Cambridge University Press, Cambridge, 1993).

[64] J. J. Thomsen, *Vibrations and Stability. Order and Chaos* (McGraw-Hill, Berkshire, 1997).

[65] P. A. Lindsay and X. Chen, *Chaos and gyrotron-type of interaction*, IEEE Trans. Plasma Sci. **22**, 834 (1994).

[66] O. Dumbrajs, R. Meyer-Spasche and A. Reinfelds, *Analysis of electron trajectories in a gyrotron resonator*, IEEE Trans. Plasma Sci. **26**, 846 (1998).

[67] O. Dumbrajs and A. Reinfelds, *Electron trajectories in a realistic gyrotron resonator*, Math. Modeling Anal. **3**, 74 (1998).

[68] N. S. Ginzburg, N. A. Zavolsky, G. S. Nusinovich and A. S. Sergeev, *Установление автоколебаний в электронных СВЧ генераторах с дифракционным выводом излучения (Self-oscillation in UHF generators with diffraction radiation output)*, Изв. Высш. Учебн. Завед. Радиофиз. **29**, 106 (1986). English translation: Radiophys. Quantum Electron. **29**, 89 (1986).

[69] N. S. Ginzburg, G. S. Nusinovich and N. A. Zavolsky, *Theory of non-stationary processes in gyrotrons with low Q resonators*, Int. J. Electron. **61**, 881 (1986).

[70] N. S. Ginzburg, N. A. Zavolsky and G. S. Nusinovich, *Динамика гиротронов с нефиксированной продольной структурой высокочастотного поля (Dynamics of gyrotrons with a variable longitudinal structure of the microwave field)*, Радиотех. Электрон. **32**, 1031 (1987). English translation: J. Comm. Technol. Electron. **32** 132 (1987).

[71] N. S. Ginzburg *et al.*, *Использование отражения с запаздыванием для получения автомодуляционных и стохастических режимов генерации в гиротронах миллиметрового диапазона (A proposal to use reflection with delay for achieving the self-modulation and stochastic regimes in millimeter-wave gyrotrons)*, Письма Ж. Тех. Физ. **24**, 53 (1998). English translation: Tech. Phys. Lett. **24**, 436 (1998).

[72] A. Grudiev, J. Jelonnek and K. Schünemann, *Time-domain analysis of reflections influence on gyrotron operation*, Phys. Plasmas **8**, 2963 (2001).

[73] A. Grudiev and K. Schünemann, *Nonstationary behavior of a gyrotron in the presence of reflections*, Int. J. Infrared Millim. Waves **24**, 429 (2003).

[74] A. Grudiev, *Numerical Study of Nonstationary Phenomena in Gyro-Oscillators*, Ph.D. thesis, Technische Universität Hamburg-Harburg, Göttingen (2003).

[75] N. A. Zavolsky, G. S. Nusinovich and A. B. Pavelyev, *Устойчивость одномодовых колебаний и нестационарные процессы в гиротронах со сверхразмерными низкодобротными резонаторами (Stability of single-mode oscillations and nonstationary processes in gyrotrons with oversized low-Q resonators)*, in *Гиротроны. Сборник научных трудов (Gyrotrons. Collected Papers)* (edited by V. A. Flyagin), pp. 84–112 (Institute of Applied Physics, Academy of Sciences of the USSR, Gorky, 1989). In Russian.

[76] N. A. Zavolsky and G. S. Nusinovich, *Нестационарные процессы в гиротроне с нефиксированной структурой ВЧ-поля (Nonstationary processes in a gyrotron with nonfixed structure of RF field)*, Радиотех. Электрон. **36**, 135 (1991). English translation in J. Comm. Technol. Electron.

[77] M. I. Airila and O. Dumbrajs, *Stochastic processes in gyrotrons*, Nucl. Fusion **43**, 1446 (2003).

[78] H. G. Schuster, *Deterministic Chaos—An Introduction* (Physik-Verlag, Weinheim, 1984).

[79] V. K. Yulpatov, Report at V Межвузовская конференция по электронике СВЧ, Саратов (The 5th Interuniversity Conference on Microwave Electronics, Saratov) (1966).

[80] V. K. Yulpatov, *Укороченные уравнения автоколебаний гиротрона (Averaged equations of oscillations in a gyrotron)*, in *Гиротрон. Сборник научных трудов (Gyrotron. Collected Papers)* (edited by A. V. Gaponov-Grekhov), pp. 26–40 (Institute of Applied Physics, Academy of Sciences of the USSR, Gorky, 1981). In Russian.

[81] V. L. Bratman, M. A. Moiseev, M. I. Petelin and R. E. Erm, *К теории гиротронов с нефиксированной структурой высокочастотного поля (Theory of gyrotrons with a nonfixed structure of the high-frequency field)*, Изв. Высш. Учебн. Завед. Радиофиз. **16**, 622 (1973). English translation: Radiophys. Quantum Electron. **16**, 474 (1973).

[82] A. W. Fliflet, M. E. Read, K. R. Chu and R. Seeley, *A self-consistent field theory for gyrotron oscillators: Application to a low Q gyromonotron*, Int. J. Electron. **53**, 505 (1982).

[83] M. I. Petelin, *Электронная селекция мод в гиротроне (Electron selection of modes in gyrotron)*, in *Гиротрон. Сборник научных трудов (Gyrotron. Collected Papers)*, pp. 77–85 (Institute of Applied Physics, Academy of Sciences of the USSR, Gorky, 1981). In Russian.

[84] M. Thumm, *State-of-the-art of high power gyro-devices and free electron masers—update 2002*, Technical Report FZKA 6815, Forschungszentrum Karlsruhe, Karlsruhe (2003).

[85] V. L. Bratman, O. Dumbrajs, P. Nikkola and A. V. Savilov, *Space charge effects as a source of electron energy spread and efficiency degradation in gyrotrons*, IEEE Trans. Plasma Sci. **28**, 633 (2000).

[86] O. Dumbrajs, P. Nikkola and B. Piosczyk, *On the negative-mass instability in gyrotrons*, Int. J. Electron. **88**, 215 (2001).

[87] V. A. Flyagin, A. V. Gaponov, M. I. Petelin and V. K. Yulpatov, *The gyrotron*, IEEE Trans. Microwave Theory Tech. **25**, 514 (1977).

[88] S. Kern, *Numerische Simulation der Gyrotron-Wechselwirkung in koaxialen Resonatoren*, Technical Report FZKA 5837, Forschungszentrum Karlsruhe, Karlsruhe (1996). In German.

[89] W. H. Press, S. A. Teukolsky, W. T. Vetterling and B. P. Flannery, *Numerical Recipes in FORTRAN. The Art of Scientific Computing* (Cambridge University Press, New York, 1994).

[90] E. Kreyszig, *Advanced Engineering Mathematics* (John Wiley & Sons, New York, 1993), seventh edition.

[91] Visual Numerics, Inc., *IMSL Math/Library, vol. 1 and 2* (1997).

[92] G. S. Nusinovich and R. E. Erm, *КПД МЦР-монотрона с гауссовым продольным распределением высокочастотного поля (Efficiency of a CRM monotron with a gaussian longitudinal distribution of high frequency fields)*, Электрон. тех. Сер. 1 Електрон. СВЧ **8**, 55 (1972). In Russian.

[93] M. I. Airila and O. Dumbrajs, *Effect of trapped electrons on gyrotron efficiency*, in *Proc. 9th Triennial ITG-Conf. "Vacuum Electronics and Displays"*, pp. 183–188, ITG-Fachbericht (VDE Verlag, Berlin, 2001).

[94] B. Piosczyk *et al.*, *2.2 MW, 165 GHz coaxial cavity gyrotron*, in *Conf. Digest, 25th Int. Conf. on Infrared and Millimeter Waves* (edited by S. Liu and X. Shen), pp. 19–20 (IEEE Press, Beijing, 2000).

[95] M. I. Airila and O. Dumbrajs, *Stochastic oscillations in gyrotrons*, in *Conf. Digest, 26th Int. Conf. on Infrared and Millimeter Waves*, pp. 5:140–5:143 (2001). Retrieved from http://www.lncmp.org/fichiers/IRMMW_2001.pdf on January 15, 2004.

[96] M. Yu. Glyavin and V. E. Zapevalov, *Reflections influence on the gyrotron oscillation regimes*, Int. J. Infrared Millim. Waves **19**, 1499 (1998).

[97] O. Dumbrajs, M. Yu. Glyavin, V. E. Zapevalov and N. A. Zavolsky, *Influence of reflections on mode competition in gyrotrons*, IEEE Trans. Plasma Sci. **28**, 588 (2000).

[98] A. Grudiev and K. Schünemann, *Nonstationary behavior of the gyrotron backward-wave oscillator*, IEEE Trans. Plasma Sci. **30**, 851 (2002).

[99] N. S. Ginzburg *et al.*, *Наблюдение автомодуляционных режимов генерации в релятивистском гиротроне с запаздывающей обратной связью (Self-modulated generation observed in a delayed feedback relativistic microwave gyrotron)*, Письма Ж. Тех. Физ. **28**, 85 (2002). English translation: Tech. Phys. Lett. **28**, 395 (2002).

[100] K. Ronald, A. W. Cross, A. D. R. Phelps and W. He, *Observations of dynamic behaviour in an electron cyclotron maser oscillator*, J. Phys. D: Appl. Phys. **34**, L17 (2001).

[101] T. H. Chang, S. H. Chen, L. R. Barnett and K. R. Chu, *Characterization of stationary and nonstationary behavior in gyrotron oscillators*, Phys. Rev. Lett. **87**, 064802 (2001).

[102] J. Hietarinta, private communication (2003).

[103] M. J. Ablowitz, C. Schober and B. M. Herbst, *Numerical chaos, roundoff errors, and homoclinic manifolds*, Phys. Rev. Lett. **71**, 2683 (1993).

[104] D. J. Kouri *et al.*, *Numerical solutions of nonlinear wave equations*, Phys. Rev. E **59**, 1274 (1999).

[105] M. J. Ablowitz, B. M. Herbst and C. M. Schober, *Discretizations, integrable systems and computation*, J. Phys. A: Math. Gen. **34**, 10671 (2001).

[106] A. V. Gaponov *et al.*, *Powerful millimeter-wave gyrotrons*, Int. J. Electron. **51**, 277 (1981).

[107] G. Dammertz *et al.*, *1 MW, 140 GHz CW gyrotron for Wendelstein 7-X*, in *Conf. Digest, 25th Int. Conf. on Infrared and Millimeter Waves* (edited by S. Liu and X. Shen), pp. 15–16 (IEEE Press, Beijing, 2000).

[108] O. Dumbrajs and L. Shenggang, *Kinetic theory of electron-cyclotron resonance masers with asymmetry of the electron beam in a cavity*, IEEE Trans. Plasma Sci. **20**, 126 (1992).

[109] T. Idehara *et al.*, *Study of electron beam misalignment in a submillimeter wave gyrotron*, Int. J. Infrared Millim. Waves **19**, 1303 (1998).

[110] E. Ott, C. Grebogi and J. A. Yorke, *Controlling chaos*, Phys. Rev. Lett. **64**, 1196 (1990).

[111] J. M. Perez, J. Steinshnider, R. E. Stallcup and A. F. Aviles, *Control of chaos in a CO_2 laser*, Appl. Phys. Lett. **65**, 1216 (1994).

Abstracts of publications 1–7

1. The Hamiltonian approach is used to analyze the equation describing the electron interaction in gyrotron resonators with realistic RF field profiles. A detailed numerical study of the behavior of electron trajectories for some specific values of parameters controlling the interaction is performed. It is found that in some cases chaos-like motions of electrons are possible.

2. The effect of electrostatic electron trapping in the presence of a depressed collector has been included in gyrotron efficiency computations. The results are presented as general contour plots in the control parameter plane. A condition for trapping is derived in terms of the retarding voltage. The overall electron efficiency as a function of the retarding voltage has been calculated for a representative set of control parameters including the effect of electron velocity spread. It is found that the onset of trapping seriously decreases the efficiency.

3. The onset of stochastic oscillations in gyrotrons is studied by means of the self-consistent theory describing nonstationary processes. Complicated alternating sequences of regions of stationary, automodulation, and chaotic oscillations are found in the plane of the generalized gyrotron variables: cyclotron resonance mismatch and dimensionless current. The results of the investigations are important in connection with attempts to increase the output power of gyrotrons by raising the current.

4. We present an extension of the self-consistent time-dependent theory describing nonstationary processes in gyrotrons to allow for reflections. Different mathematical descriptions of partial reflection of the output signal are compared, and numerical algorithms for analyzing them are given. Using a novel description, we have computed a map of gyrotron oscillations, which identifies the regimes of stationary, periodically modulated and chaotic oscillations in the plane of generalized gyrotron variables when reflection is present. In general, reflections drive the gyrotron into quasiperiodic oscillations instead of chaos, but also the threshold current for chaotic oscillations decreases somewhat. The results can be exploited in the development of high-power gyrotrons for electron cyclotron resonance heating (ECRH) and electron cyclotron current drive (ECCD) of fusion plasmas, but also in low-power applications, where stochastic oscillations might be useful.

5. Influence of reflections on the operation of the 2 MW, CW 170 GHz coaxial cavity gyrotron oscillating in the $\mathrm{TE}^{-}_{34,19}$ mode is studied. In particular, frequency-independent power reflections, *e.g.*, from plasma or some elements of the transmission line, larger than 1% and occurring in a poor phase may lead to oscillation breakdown and should be avoided. Frequency-dependent reflections from a specially designed diamond window influence mode competition, but contract the oscillation region of the operating mode noticeably only under the unrealistic assumption that all reflected power returns to the cavity. The conclusion is that the gyrotron is sufficiently robust against possible negative effects related to reflections.

6. Nonstationary oscillations in gyrotrons are investigated for large azimuthal indices of modes leading in the transverse section of gyrotron resonators to spatial chaos in azimuthal direction. Limiting values of the azimuthal index m of the mode, beyond which stationary single-mode operation of a gyrotron becomes impossible, are found.

7. The two-dimensional self-consistent time-dependent theory of beam-wave interaction in gyrotron resonators has been modified to account for eccentricity of the annular hollow electron beam. Numerical analysis yields the effect of beam eccentricity on the previously known limiting values of the azimuthal index of the mode, beyond which stationary single-mode operation becomes impossible.